Cell

A Phosphorylation Cycle Shapes Gradients of the DYRK Family Kinase Pom1 at the Plasma Membrane

Olivier Hachet,[1] Martine Berthelot-Grosjean,[1,2] Kyriakos Kokkoris,[1] Vincent Vincenzetti,[1] Josselin Moosbrugger,[1] and Sophie G. Martin[1,*]

[1]Department of Fundamental Microbiology, Faculty of Biology and Medicine, University of Lausanne, CH-1015 Lausanne, Switzerland
[2]Present address: Centre des Sciences du Goût et de l'Alimentation, UMR-6265 CNRS, UMR-1324 INRA, Université de Bourgogne, Agrosup Dijon, 21000 Dijon, France
*Correspondence: sophie.martin@unil.ch
DOI 10.1016/j.cell.2011.05.014

SUMMARY

Concentration gradients regulate many cell biological and developmental processes. In rod-shaped fission yeast cells, polar cortical gradients of the DYRK family kinase Pom1 couple cell length with mitotic commitment by inhibiting a mitotic inducer positioned at midcell. However, how Pom1 gradients are established is unknown. Here, we show that Tea4, which is normally deposited at cell tips by microtubules, is both necessary and, upon ectopic cortical localization, sufficient to recruit Pom1 to the cell cortex. Pom1 then moves laterally at the plasma membrane, which it binds through a basic region exhibiting direct lipid interaction. Pom1 autophosphorylates in this region to lower lipid affinity and promote membrane release. Tea4 triggers Pom1 plasma membrane association by promoting its dephosphorylation through the protein phosphatase 1 Dis2. We propose that local dephosphorylation induces Pom1 membrane association and nucleates a gradient shaped by the opposing actions of lateral diffusion and autophosphorylation-dependent membrane detachment.

INTRODUCTION

Concentration gradients regulate various cell biological and developmental processes, ranging from mitotic spindle organization to body patterning. Biological gradients are best understood during development, when morphogen gradients translate cell position into distinct cell fate, depending on local morphogen concentration. Gradients also occur at much smaller scales within cells, where they impart spatial cellular order. For instance, gradients of Ran-GTP and phospho-stathmin regulate mitotic spindle formation around chromatin, Aurora B gradients control cytokinesis, and gradients of MinD, MipZ, and Pom1 provide spatial control on cell division in various prokaryotes and eukaryotes (Fuller, 2010; Lutkenhaus, 2007). A defining feature of gradients is their potential to communicate information over long distances, for which gradient shape should be carefully monitored. Thus, understanding the molecular mechanisms underlying gradient formation is crucial. Here, we have dissected the mechanisms of gradient formation of the DYRK family kinase Pom1 in fission yeast.

Schizosaccharomyces pombe cells are rod-shaped, grow by cell tip extension, and divide by medial fission. Spatial order is conferred by a system of antiparallel microtubules aligned along the length of the cell and nucleated from nuclear-associated organizing centers. Microtubules serve to position the nucleus to the geometric middle of the cell and transport a pair of landmark proteins, Tea1 and Tea4, to cell ends (Chang and Martin, 2009; Martin et al., 2005; Mata and Nurse, 1997; Tatebe et al., 2005). In turn, these landmarks recruit Pom1 to cell ends, from where this protein forms concentration gradients (Bähler and Pringle, 1998; Padte et al., 2006; Tatebe et al., 2005). These three proteins regulate cell morphology and bipolar growth, in part by allowing Cdc42 activation and recruiting actin nucleation factors to cell tips (Martin et al., 2005; Tatebe et al., 2008). Tea4 also directly associates with and recruits the protein phosphatase 1 (PP1) Dis2 to cell tips (Alvarez-Tabarés et al., 2007). Dis2 is one of only two PP1 catalytic subunits in *S. pombe* and is recruited to many cellular locations by specific regulatory factors. Tea1, Tea4, and Pom1 also impart negative signal to prevent cell division at cell tips (Almonacid et al., 2009; Celton-Morizur et al., 2006; Huang et al., 2007; Padte et al., 2006). Together with positive signals conferred by the nucleus through the protein Mid1 (Almonacid et al., 2009), negative signals from cell tips define the position of cell division at midcell.

In addition to Pom1's roles in bipolar growth, cell morphogenesis, and septum positioning, we and others recently discovered that this kinase functions as a dose-dependent inhibitor of entry into mitosis (Martin and Berthelot-Grosjean, 2009; Moseley et al., 2009). Pom1 negatively regulates an activator of mitotic entry, the protein kinase Cdr2. While Pom1 forms polar gradients, Cdr2 localizes to a cortical band placed at the cell equator (Morrell et al., 2004). The observation that Pom1 concentration at midcell is higher in short than long cells suggested a model where Pom1 inhibits Cdr2 until the cell has reached a sufficient length. Accordingly, experiments in which Pom1 was ectopically localized at the cell equator led to a delay of mitosis and the formation of elongated

cells. Thus, Pom1 gradients form a cell length-monitoring system for coordinating mitotic commitment with cell growth.

Pom1 is part of the DYRK (*d*ual-specificity t*y*rosine-*r*egulated *k*inase) family of kinases conserved in eukaryotes. These kinases self-catalyze the phosphorylation of tyrosines in their activation loop in an autophosphorylation reaction that occurs on a DYRK translational intermediate (Lochhead et al., 2005). Mature DYRKs do not phosphorylate tyrosines but can phosphorylate substrates on serines and threonines. In vitro work on mammalian DYRK1a, DYRK2, and DYRK3 has shown that phosphorylation occurs preferentially within the consensus $RX_{(1-3)}$[ST][PVL] (Campbell and Proud, 2002; Himpel et al., 2000), although several DYRK substrates show considerable variation relative to this consensus (Aranda et al., 2011). Although the specific substrates of each DYRK diverge widely and are still poorly defined, a common function of this family may be coordination of cell cycle, cell growth, and differentiation (Aranda et al., 2011).

To understand how the Pom1 length-sensing device works for cell size homeostasis, we asked how Pom1 gradients are established. Our experiments were guided by two previously known pieces of information: first, Tea1 and Tea4 are essential for the localization of Pom1 to cell tips (Bähler and Pringle, 1998; Celton-Morizur et al., 2006; Padte et al., 2006; Tatebe et al., 2005); and second, Pom1 distribution depends on its activity because a kinase-dead version of Pom1 localizes indiscriminately around the entire cell periphery (Bähler and Nurse, 2001). We demonstrate a simple mechanism underlying the formation of cortical concentration gradients of Pom1, which are nucleated by local Tea4-mediated dephosphorylation and shaped by lateral movement and autocatalytic activity.

RESULTS

Tea4 Is Necessary and Sufficient to Nucleate Pom1 Gradients at the Cell Cortex

Pom1-GFP gradients have previously been measured in projections of the entire cell volume including both cytoplasmic and cortical compartments onto a single line. Confocal sectioning suggests that these gradients are primarily cortical (Figure 1A and Figure S1A available online). This can be illustrated by measuring the fluorescence along lines drawn at the cell cortex or across the length of the cell. Whereas the latter shows a uniform low concentration of Pom1 in the cytoplasm, the fluorescence profile along the cell cortex reveals gradients of Pom1 with highest concentration at cell tips. We note that these gradients are not completely smooth but that clusters of higher intensity are visible at the cortex.

We envisaged a simple model where Pom1 concentration gradients are established by protein transport/trapping and lateral movement. The microtubule-associated polarity landmarks Tea1 and Tea4 are required for Pom1 localization (Bähler and Pringle, 1998; Celton-Morizur et al., 2006; Padte et al., 2006; Tatebe et al., 2005). In a limited screen through polarity mutants, we found that *tea1Δ* and *tea4Δ* were the only mutants to robustly affect Pom1-GFP localization (Figures S1B and S1C). Pom1 failed to localize to the cell cortex in *tea4Δ* cells, except for weak residual localization at the division site, and instead appeared cytoplasmic. In *tea1Δ* cells in contrast, in which Tea4 fails to localize to cell ends (Martin et al., 2005; Tatebe et al., 2005), weak cortical localization of Pom1 was observed (Padte et al., 2006) (Figure S1B). Thus, we focused our attention on Tea4. Measurement of Tea4-GFP and Pom1-GFP distributions at cell tips showed that these are distinct: Pom1 exhibits a wider cortical localization than Tea4 (Figure 1B, far right). Similarly, Tea4-GFP and Pom1-tdTomato imaged in double-tagged strains do not precisely overlap: whereas Tea4 is restricted to the tips of the cells, Pom1 spreads further along cell sides (Figure 1B). Importantly, Pom1-tdTomato exhibits the same localization pattern as Pom1-GFP (Figure 1B, far right panel), indicating that different fluorophores do not influence the observed patterns of Pom1 localization. This differential distribution suggests that Tea4 may recruit Pom1 to cell tips from where Pom1 moves in the plane of the membrane.

To visualize Pom1 lateral movement, we photobleached Pom1-GFP at half-cell tips (Figure 1C). Recovery of signal occurred faster at the edges of the bleached region, indicating movement from the adjacent fluorescent half. Fluorescence recovery after photobleaching (FRAP) experiments on inactive $Pom1^{KD}$-GFP, which localizes around the entire cell cortex (Bähler and Nurse, 2001), confirmed this behavior. Here, we photobleached the entire midsection of the cell (Figure 1D). Again, we detected nonuniform recovery of fluorescence suggestive of movement from the adjacent nonbleached zone. Thus, Pom1 moves laterally at the plasma membrane.

These results suggest that recruitment of Pom1 by Tea4 at cell tips and lateral movement are key elements for the formation of Pom1 gradients. To test whether these are sufficient to generate Pom1 gradients, we ectopically localized Tea4 by generating a fusion between the spindle pole body (SPB) component Ppc89, GFP, and Tea4 and expressing it in *tea4Δ pom1-tdTomato* cells. Ppc89-GFP-Tea4 mimicked the localization patterns of both Ppc89 and Tea4 to the SPB and cell ends, respectively. This fusion also unexpectedly formed ectopic foci along cell sides. Pom1-tdTomato was recruited to cell ends and to these ectopic lateral foci, but not to the SPB (Figure 1E). Measurement of the distribution of these proteins suggested that, whereas the Ppc89-GFP-Tea4 fusion formed tight dots, Pom1-tdTomato spread further along the plane of the membrane (Figure 1F, a), indicating the formation of local cortical Pom1 gradient. In contrast, control measurements perpendicular to the plane of the membrane showed nearly identical distribution of Tea4 and Pom1 along this axis (Figure 1F, b). Thus, Tea4 is not only necessary but also sufficient to nucleate the formation of a Pom1 gradient anywhere along the cell cortex.

Below, we dissect three key elements in the formation of Pom1 gradients: how Pom1 associates with the cell cortex; how this association is modulated by kinase activity; and finally, how Tea4 mediates Pom1 recruitment to cell tips.

Pom1 Binds Lipids

To map the region of Pom1 required for cortex localization, we generated a series of GFP-tagged truncations of Pom1 on plasmids and observed their localization in *pom1Δ* cells (Figures 2A–2C). Truncation of the first 305 amino acids had no apparent effect on Pom1 localization. Pom1 lacking the first 419 residues still localized to the cortex, albeit less efficiently. In contrast,

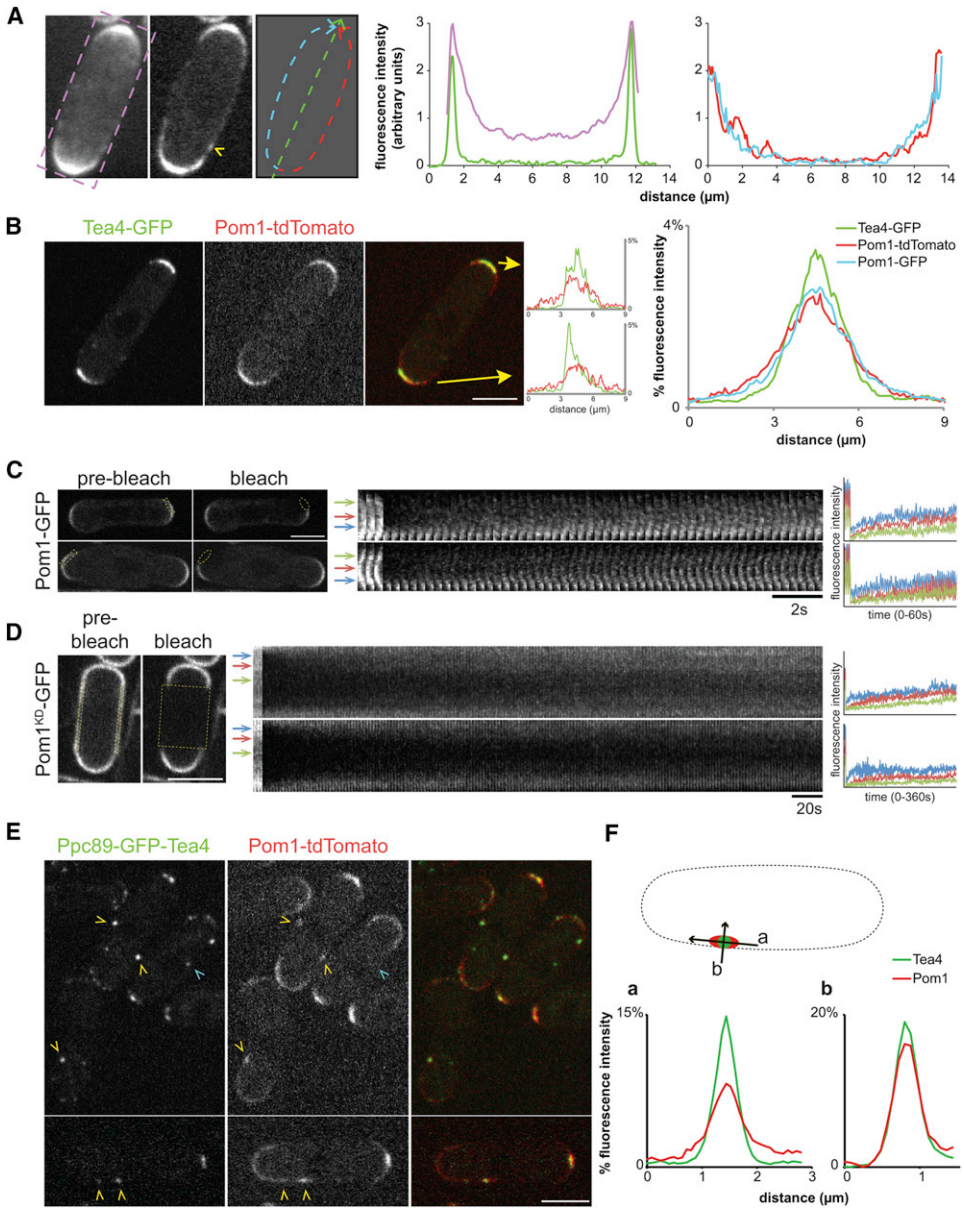

Figure 1. Tea4 Is Sufficient to Nucleate a Cortical Pom1 Gradient

(A) Sum projection (left) and single medial confocal section (right) of Pom1-GFP. The purple line represents the total cellular measure of Pom1-GFP fluorescence intensity projected onto a single line. Green, red, and blue lines represent measures on the medial confocal section, as shown. The yellow arrowhead labels a Pom1-GFP cluster at the cell cortex.

(B) Localization of Tea4-GFP and Pom1-tdTomato in the same cell. The profile of fluorescence intensity along the periphery of both cell ends is shown on the right. The far-right graph shows an average over 16 such measurements, as well as measurements of Pom1-GFP distribution as shown in (A). To compare fluorescence distribution, the integrated fluorescence intensity for each curve was normalized to one, and percentage of this total is shown on the graphs.

(C and D) Kymographs of FRAP at the lateral cortex of Pom1-GFP and Pom1^{KD}-GFP expressed from plasmids. The cells on the left show the prebleach and bleach time points. Boxes represent the regions used in the kymographs and the bleach zone, respectively. Graphs show the fluorescence profile along lines drawn on the kymographs at the levels of the colored arrows. Note that recovery occurs preferentially from the edges of the bleached region.

(E) Ppc89-GFP-Tea4 recruits Pom1-tdTomato to the lateral cortex, but not the nuclear membrane. Yellow arrowheads denote lateral localization of Ppc89-GFP-Tea4 and Pom1-tdTomato. Blue arrowhead shows SPB localization of Ppc89-GFP-Tea4 and absence of Pom1-tdTomato. Scale bars, 5 μm.

(F) Distribution of Ppc89-GFP-Tea4 and Pom1-tdTomato along (a) and perpendicular to (b) the lateral plasma membrane. Average of 30 measurements is shown. Curves were normalized as in (B).

See also Figure S1.

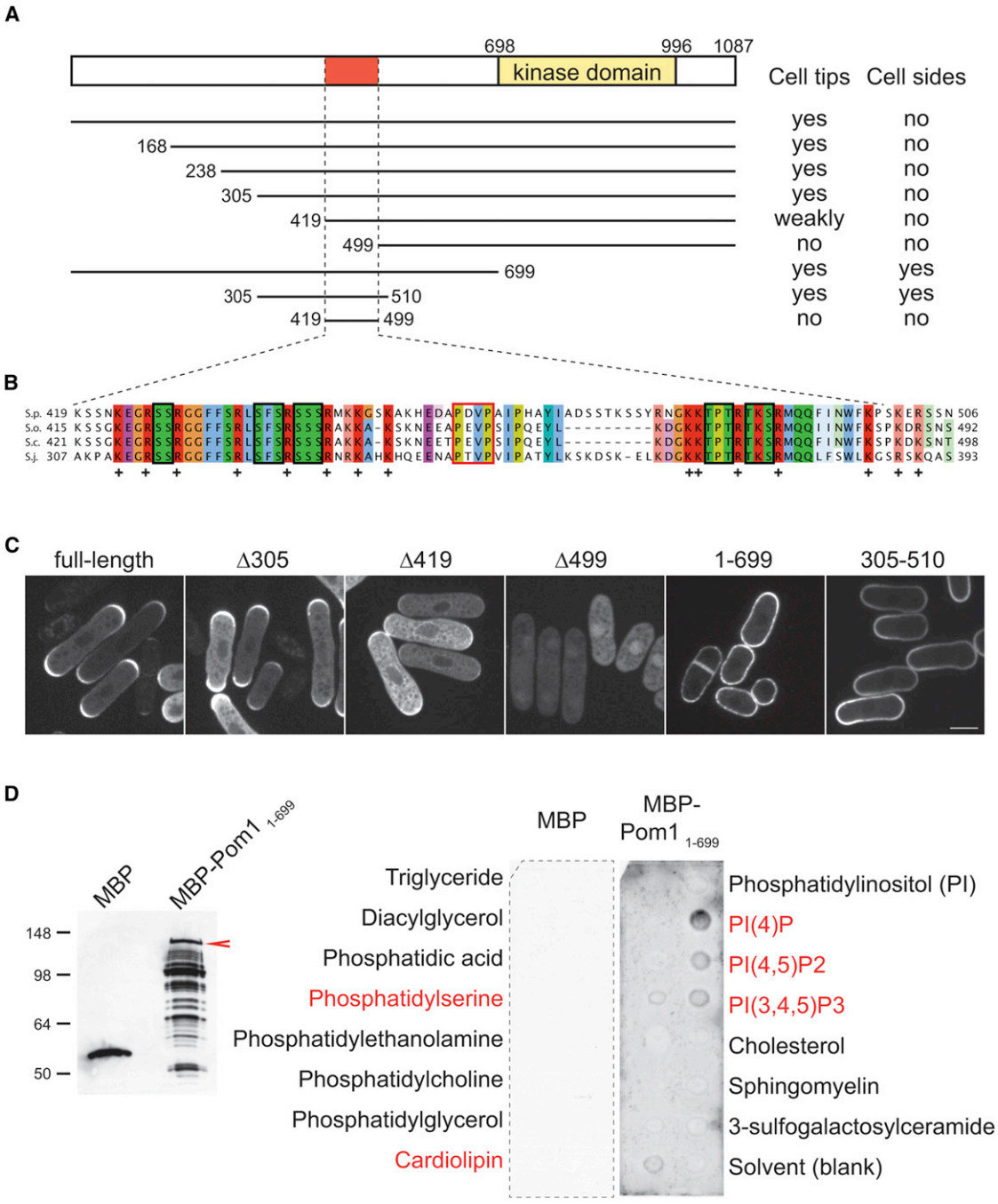

Figure 2. A Positively Charged Region of Pom1 Mediates Lipid Binding

(A) Schematic representation of Pom1 and truncation fragments. These were tagged with GFP, expressed from plasmids in *pom1Δ* cells and imaged. Description of their localization is detailed on the right.

(B) Alignment of the region necessary for cortical binding between Pom1 orthologs in four *Schizosaccharomyces* species: S.p., *pombe*; S.o., *octosporus*; S.c., *cryophobus*; and S.j., *japonicus*. Conserved basic residues are highlighted in red and by plus (+) signs. Black squares box serine/threonine residues mutated to alanine in the Pom1^{6A} allele. The red square boxes proline residues mutated to alanine in the Pom1$^{5PxxP'}$ allele.

(C) Localization of selected constructs as described in (A). Scale bar, 5 μm.

(D) Protein-lipid overlay assay with MBP and MBP-Pom1$_{1–699}$. Loading control is shown as anti-MBP western blot on the left. Full-length MBP-Pom1$_{1–699}$ fragment is labeled by red arrowhead. Lower bands likely represent breakdown products. Lipids spotted on each side of both membranes are indicated on the left and right, respectively. Lipids to which MBP-Pom1$_{1–699}$ shows significant association are shown in red. Both blots were treated in parallel using identical conditions throughout.

See also Figure S2.

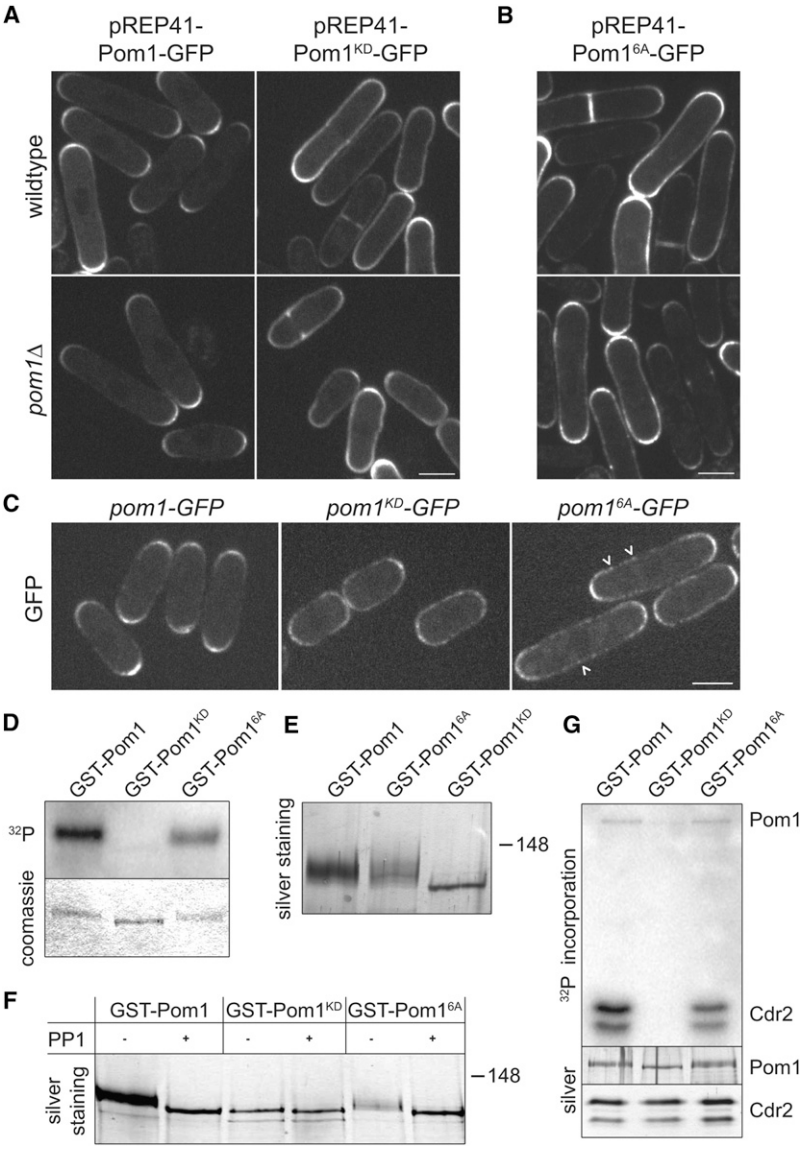

Figure 3. Autophosphorylation of Pom1 Restricts Its Cortical Localization to Cell Tips

(A) Localization of Pom1-GFP and inactive Pom1^{KD}-GFP expressed from plasmids in wild-type and *pom1Δ* strains.

(B) Localization of nonphosphorylatable Pom1^{6A}-GFP expressed from plasmids in wild-type and *pom1Δ* strains.

(C) Localization of Pom1-GFP, Pom1^{KD}-GFP, and Pom1^{6A}-GFP integrated as sole copy at the endogenous *pom1* locus. Arrowheads label a few Pom1^{6A}-GFP clusters at the cell cortex. Scale bars, 5 μm.

(D) In vitro kinase assay on recombinant GST-Pom1, GST-Pom1^{KD}, and GST-Pom1^{6A}. Top panel shows phosphorimager detection of ^{32}P incorporation; bottom panel shows Coomassie-stained gel.

(E) Side-by-side comparison of the migration patterns of GST-Pom1, GST-Pom1^{6A}, and GST-Pom1^{KD}.

(F) Migration pattern of recombinant GST-Pom1, GST-Pom1^{KD}, and GST-Pom1^{6A} with or without PP1 treatment. Silver-stained gel is shown.

(G) In vitro kinase assay of recombinant GST-Pom1, GST-Pom1^{KD}, and GST-Pom1^{6A} with 6His-Cdr2$_{423–532}$ as substrate. Top panel shows phosphorimager detection of ^{32}P incorporation; bottom panels show silver-stained gels. See also Figure S3.

deleting the first 499 residues prevented cortex localization, defining amino acids 419–499 as essential for cortical localization. Pom1 fragments containing this region but lacking the kinase domain (i.e., Pom1$_{1–699}$ and Pom1$_{305–510}$) localized efficiently to the cell cortex but were not restricted to cell ends (see below). However, we note that the fragment 419–499 was not sufficient for cortical localization. Sequence alignment showed that this region was well conserved between Pom1 and orthologs in other *Schizosaccharomyces* species (Figure S2 and Figure 2B).

This region is rich in arginine and lysine residues (19 out of 81 residues) and, thus, highly positively charged, suggesting that it may bind negatively charged lipids directly through electrostatic interactions. Indeed, recombinant Pom1 N-terminus (MBP-Pom1$_{1–699}$) was able to bind directly to several, but not all, negatively charged lipids, namely phosphatidylserine, phosphatidylinositol phosphates, and cardiolipin in a protein-lipid overlay assay (Figure 2D). Phosphatidylserine and phosphatidylinositol phosphates are components of the plasma membrane. Cardiolipin is mostly found in the inner mitochondrial membrane, and so it is unclear whether this interaction exists in vivo. We also note that, probably due to its high global positive charge (+15.5 for MBP-Pom1$_{1–699}$, +25 for Pom1$_{1–699}$ at pH 7), MBP-Pom1$_{1–699}$ bound the nitrocellulose membrane, resulting in significant background. Together, these experiments suggest that Pom1 directly associates with lipids at the plasma membrane through its basic region.

Pom1 Autophosphorylates to Restrict Its Localization to Cell Tips

Investigation of a kinase-dead allele of *pom1* (*pom1-2*; here labeled *pom1^{KD}*) has previously shown that Pom1 kinase activity modulates its localization: in contrast to Pom1-GFP localization to cell tips, Pom1^{KD}-GFP expressed as sole copy from the endogenous promoter localizes indiscriminately around the entire cell cortex (Bähler and Nurse, 2001) (see also Figure 3C). We confirmed this observation by expressing Pom1^{KD}-GFP from plasmids in *pom1Δ* cells. Importantly, when expressed in wild-type cells, Pom1^{KD}-GFP was also mislocalized around the entire cortex, indicating that the endogenous wild-type Pom1 activity, though competent for regulating cell morphogenesis and size, was not able to restore correct localization to the inactive kinase (Figure 3A). Similarly, expression of wild-type untagged Pom1 from plasmids in *pom1^{KD}-GFP* cells was unable to restore the localization of endogenous Pom1^{KD}-GFP to cell tips (data not shown). These data suggest that Pom1 autophosphorylates to restrict its localization to cell tips.

Work on mammalian DYRKs has defined a loose phosphorylation consensus site $RX_{(1-3)}$[ST][PVL] (Campbell and Proud, 2002; Himpel et al., 2000). We hypothesized that Pom1 phosphorylates similar sites and looked for conserved candidate autophosphorylation sites in the Pom1 sequence using the degenerate simplified [RK]$X_{(1-3)}$[ST] motif. This identified 15 candidate sites. We focused on those located outside the kinase domain and in well-conserved regions of the proteins and mutated up to six to alanine to generate Pom1^{1A}–Pom1^{6A}. (Note that one site can include one to three serines or threonines that we mutated simultaneously.) Five of these sites were in the region mediating lipid binding defined above (Figure S2 and Figure 2B). Expression of Pom1^{1A}-GFP to Pom1^{6A}-GFP on plasmids in *pom1Δ* cells showed a progressive spreading of the kinase along the cortex of the cells (Figure S3). Pom1^{6A}-GFP recapitulated the largely homogeneous cortical localization observed for Pom1^{KD}-GFP in either wild-type or *pom1Δ* cells (Figure 3B). We note that strong overexpression of Pom1^{6A}-GFP produces morphological abnormalities, a phenotype also observed upon overexpression of wild-type but not the kinase-dead allele (Bähler and Nurse, 2001) (Figure S3). This suggests that Pom1^{6A} is an active kinase. We tested more stringently the localization of the *pom1^{6A}* allele by integrating it at the endogenous locus as sole copy of *pom1*. Pom1^{6A}-GFP expressed under endogenous promoter also localized around the entire cortex, displaying numerous clusters of Pom1 scattered around the cell periphery, similar to inactive Pom1^{KD} (Figure 3C). This localization is consistent with the idea that these six sites represent targets of autophosphorylation.

To confirm biochemically that Pom1 autophosphorylates, we purified recombinant full-length Pom1 and Pom1^{KD} and performed in vitro kinase assays (Figure 3D). A significant amount of ^{32}P was incorporated by wild-type, but not kinase-dead Pom1. We also noticed that Pom1 migrated more slowly than Pom1^{KD} on SDS-PAGE (Figure 3E). Treatment of Pom1 with commercial PP1 abolished this slow migration but did not change the Pom1^{KD} migration pattern, indicating that recombinant Pom1 is autophosphorylated in the bacterial cell (Figure 3F). Similar assays with Pom1^{6A} showed an intermediate behavior, where Pom1^{6A} incorporated less ^{32}P and migrated at levels intermediate between wild-type and kinase-dead Pom1 (Figures 3D–3F). This shows that Pom1^{6A} is active and that the mutated sites likely represent some but not all autophosphorylation sites. Pom1^{6A} was also active in kinase assays with Cdr2 fragment as substrate, indicating that it remains competent in phosphorylating a known exogenous substrate (Figure 3G) (Martin and Berthelot-Grosjean, 2009). We subsequently identified all autophosphorylation sites on recombinant wild-type Pom1 by mass spectrometry. This analysis identified a total of 41 autophosphorylation sites and confirmed that 2 of the 6 mutated sites were indeed autophosphorylated (Figure S2). This analysis unfortunately did not inform about the phosphorylation status of the four other sites, which were not covered by any peptide identified by mass spectrometry, despite extensive effort and sequence coverage of over 95% (see Extended Experimental Procedures and Figure S2). In summary, Pom1 is heavily autophosphorylated, and partly unphosphorylated Pom1^{6A} is not restricted to the cell tip cortex and disrupts Pom1 gradients.

Pom1 Autophosphorylation Weakens Membrane Binding

To explore the dynamics of Pom1 autophosphorylation, we made use of the *pom1-as1* allele, which encodes an ATP analog-sensitive Pom1 form that can be inhibited by addition of the chemical inhibitor 1NM-PP1 (Padte et al., 2006). Under normal growth conditions, Pom1-as1-tdTomato localizes correctly to the cell tip cortex. However, within 1–2 min of 1NM-PP1 addition, Pom1-as1-tdTomato was delocalized around the entire cell periphery (Figure 4A). This fast delocalization suggests that inactivated Pom1-as1 is rapidly dephosphorylated. An alternative possibility is that phospho-Pom1 may be rapidly degraded and resynthesized. However, we found that inhibition of protein translation with cycloheximide or disruption of protein degradation in proteasome mutants did not significantly affect the levels and distribution of Pom1 even after several hours (Figure S4), suggesting that Pom1 protein is stable over a significantly longer time. Thus, kinase activity is continuously required to antagonize dephosphorylation and prevent Pom1 localization along the lateral cortex.

Using FRAP experiments, we determined the turnover of Pom1 at the cell cortex (Figures 4B and 4C). We photobleached one entire cell tip to measure the exchange between cortical and cytoplasmic Pom1-GFP. Wild-type Pom1-GFP recovered with an estimated half-time of about 60 s. Inactive Pom1^{KD}-GFP and nonphosphorylatable Pom1^{6A}-GFP also recovered but with significantly slower half-time of over 120 s. Reduced exchange of these alleles suggest that unphosphorylated Pom1 alleles are more stable at the membrane and may also reflect their lower abundance in the cytoplasm. In agreement with these results, recombinant full-length Pom1, which autophosphorylates in bacteria, bound phospholipids in vitro with significantly higher affinity after dephosphorylation (Figure 4D). Dephosphorylated Pom1 also bound the nitrocellulose membrane, resulting in high background signal, similar to MBP-Pom1$_{1-699}$ tested above. Again, this may be due to the high global positive charge of Pom1 (+22.5 for MBP-Pom1, +32 for Pom1 at pH 7), which is likely abolished upon autophosphorylation at over 40 potential sites. We also note a slight change in the lipid specificity of Pom1: autophosphorylated Pom1 bound phosphatidic acid, a rare phospholipid in *S. pombe* (Koukou et al., 1990), whereas this phospholipid was not bound by the dephosphorylated form of Pom1. In summary our results suggest that Pom1 binds the plasma membrane directly when nonphosphorylated and that autophosphorylation weakens this interaction.

Pom1 Binds Tea4

We showed above that Tea4 is both necessary and sufficient to nucleate Pom1 gradient formation. Tea4 is an SH3 domain-containing protein. Direct interactions have been described with Tea1, the formin For3, the PP1 Dis2, and the MAPKKK Win1, none of which involves the SH3 domain (Alvarez-Tabarés et al., 2007; Martin et al., 2005; Tatebe et al., 2005). In two-hybrid assays we found that Tea4 binds Pom1 through its SH3 domain because complete deletion or point mutation in the ligand-binding interface of the SH3 domain abolished this interaction (Figure 5A). This interaction occurs in vivo, as Tea4-HA was coimmunoprecipitated with Pom1-GFP (Figure 5B). Again, point

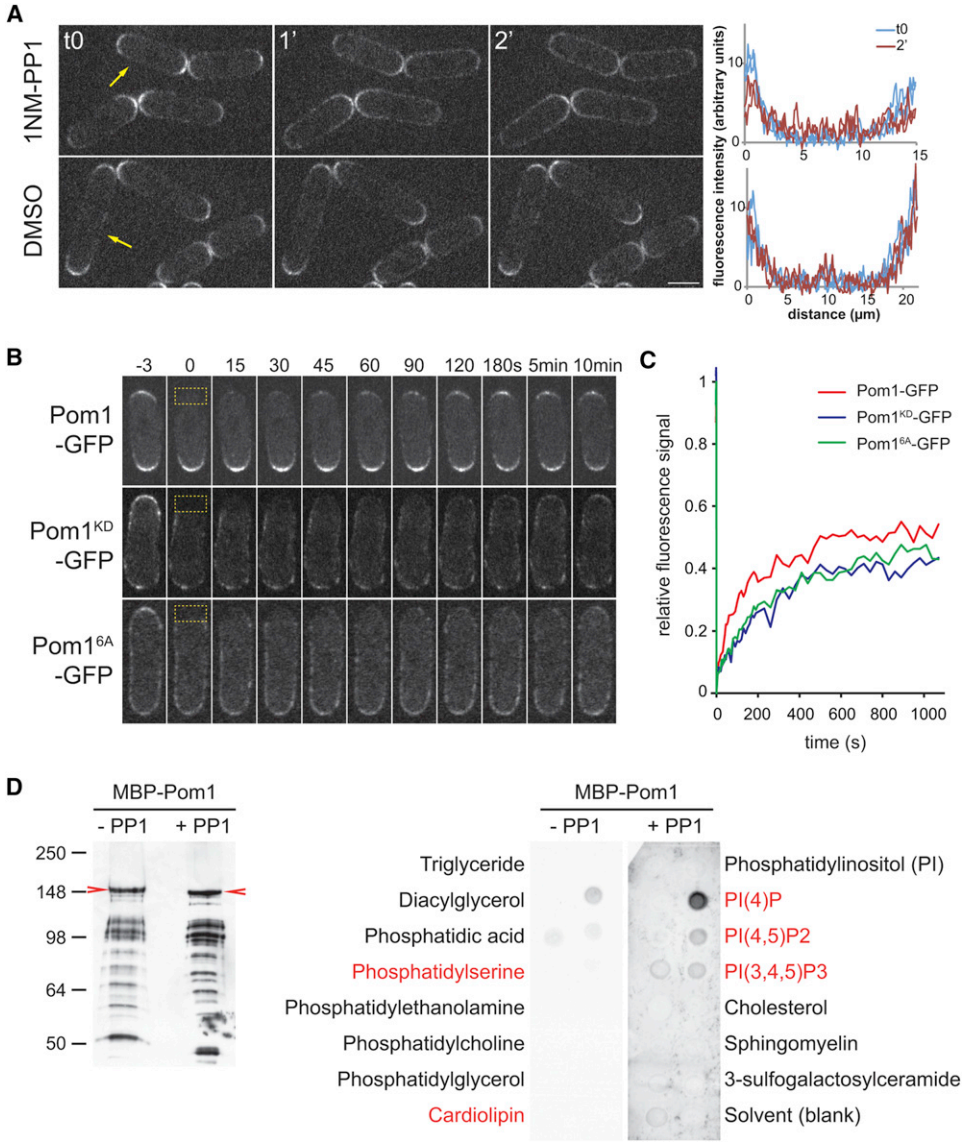

Figure 4. Pom1 Activity Modulates Membrane Attachment

(A) Localization of Pom1-as1-tdTomato before and after 1–2 min treatment with 20 μM 1NM-PP1 or DMSO. Scale bar, 5 μm. Arrows indicate cells for which the profile of fluorescence intensity along the periphery of both cell sides at 0 and 2 min is shown on the right.

(B) FRAP of Pom1-GFP, Pom1^{KD}-GFP, and Pom1^{6A}-GFP. The bleached region at cell tips is boxed.

(C) Quantification of FRAP experiments as shown in (B). Each curve represents an average of five experiments.

(D) Protein-lipid overlay assay with MBP-Pom1, with or without PP1 treatment. Loading control is shown as anti-MBP western blot on the left. Full-length proteins are labeled with red arrowheads. Lower bands likely correspond to breakdown products. Note the faster migration of most fragments in the PP1-treated sample. Lipids to which dephosphorylated MBP-Pom1 shows significant association are shown in red. Both blots were treated in parallel using identical conditions throughout.

See also Figure S4.

mutations in the Tea4 SH3 domain (Tea4$^{SH3^*}$) abolished this interaction. In contrast, point mutations in the motif shown to mediate binding to Dis2 (Tea4$^{RVxF^*}$) did not block Tea4-Pom1 interaction (Alvarez-Tabarés et al., 2007). The Tea4-Pom1 interaction was also not dependent on Pom1 activity or phosphorylation status, as Tea4 was coimmunoprecipitated with Pom1^{KD}. SH3 domains often bind polyproline motifs. Sequence alignment revealed five such conserved motifs in Pom1 (Figure S2). We sequentially mutated two prolines to alanines in each of these to create a Pom1$^{5PxxP^*}$ mutant. These mutations also impaired Tea4 binding in coimmunoprecipitation experiments (Figure 5B). We conclude that Tea4 and Pom1 bind to each other through SH3-PxxP interactions.

Pom1-GFP localization was dramatically affected by disruption of its interaction with Tea4. In *tea4$^{SH3^*}$* cells, Pom1-GFP was cytoplasmic, like in *tea4Δ* cells (Figure 5C). Mutation of

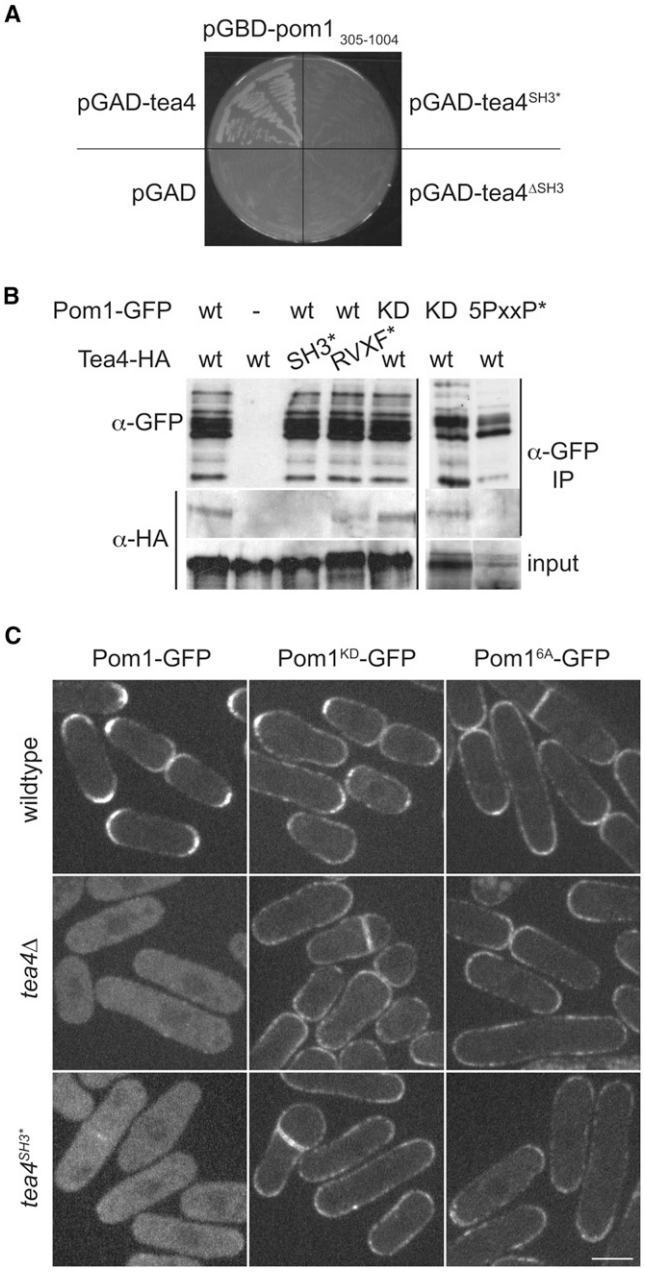

Figure 5. Tea4 Binds Pom1 and Is Required for the Localization of Wild-Type, but Not Dephosphorylated, Pom1

(A) Two-hybrid interaction between indicated constructs of Tea4 and Pom1. Growth on SD medium lacking histidine is shown.

(B) Coimmunoprecipitation of Tea4-HA with Pom1-GFP. Tea4 and Pom1 alleles are indicated at the top. The bottom lane shows Tea4-HA input. The first five and the last two lanes were obtained in distinct experiments. The last two were on the same gel, but not side by side. Note that the patterns of Pom1 breakdown products are similar in strains of distinct genotypes.

(C) Localization of Pom1-GFP, Pom1^{KD}-GFP, and Pom1^{6A}-GFP in wild-type, *tea4Δ*, and *tea4^{SH3*}* cells, as indicated. Scale bar, 5 μm.

See also Figure S5.

the Pom1 PxxP motifs also increased cytoplasmic Pom1 and reduced Pom1 localization to the cell cortex but did not completely abolish it (Figure S5). Even when Pom1^{5PxxP*}-GFP was expressed at the endogenous genomic locus, residual cortical localization at cell tips was observed, suggesting that the *tea4^{SH3*}* and *pom1^{5PxxP*}* mutations are not equivalent (see Figure 6F and below).

Tea4 Plays a Regulatory, Nonstoichiometric Role in Pom1 Localization

We investigated the localization of inactive Pom1^{KD} and unphosphorylatable Pom1^{6A} in *tea4* mutant cells. Unexpectedly, both alleles localized efficiently to the cell periphery in *tea4Δ* and *tea4^{SH3*}* mutant cells (Figure 5C). In fact, even mutation of one or only a few autophosphorylation sites was sufficient to restore some cortical localization to Pom1 in *tea4Δ* cells (Figure S6). Similarly, inactivating Pom1^{5PxxP*} by constructing a Pom1$^{KD\text{-}5PxxP*}$ allele restored efficient cortical localization to this allele (Figure 6A). This indicates that Tea4 binding is not required to localize inactive, unphosphorylated Pom1 to the cell cortex. These results strongly suggest that Tea4 does not act as a physical anchor at the cortex but fulfills a regulatory function.

In agreement with this hypothesis, we observed that amounts of Tea4 below detection levels were sufficient to ensure proper localization of Pom1 (Figure 6B). Here, Tea4-GFP was expressed under repressible promoter in *tea4Δ pom1-tdTomato* cells. Promoter repression reduced Tea4 levels below detection but still allowed correct Pom1 localization. Thus, Tea4 is unlikely to act as a stoichiometric anchor for Pom1 at the cortex.

Tea4 Promotes Pom1 Dephosphorylation at Cell Tips

Tea4 acts as a PP1 regulatory subunit by recruiting the phosphatase Dis2 to cell tips (Alvarez-Tabarés et al., 2007). We tested the hypothesis that Tea4 mediates the PP1-dependent dephosphorylation of Pom1 at cell tips. In agreement with this idea, we have shown above that recombinant, autophosphorylated Pom1 is dephosphorylated by PP1 (Figure 3F). We first verified the interaction of Tea4 with Dis2. Tea4-HA was readily coimmunoprecipitated with GFP-Dis2 in wild-type cells (Figure 6C). As previously described, this interaction was dependent on the Tea4 RVxF motif (Alvarez-Tabarés et al., 2007). We also found that the integrity of the Tea4 SH3 domain was essential for this interaction. Indeed, both Tea4^{RVxF*} and Tea4^{SH3*} failed to coimmunoprecipitate with GFP-Dis2 (Figure 6C). We note that the RVxF* mutation may not block Dis2 binding completely, as minor amounts of Tea4^{RVxF*} could be detected in the Dis2 immunoprecipitate upon long exposure (data not shown). Accordingly, GFP-Dis2 was delocalized from cell tips (but not from other locations) in *tea4Δ*, *tea4^{RVxF*}*, and *tea4^{SH3*}* mutants, but not in *pom1Δ* backgrounds (Figure 6D).

By using the bimolecular fluorescence complementation (BiFC) technique, where two halves of YFP fused to distinct proteins reform an intact fluorescent complex upon interaction (Kerppola, 2006), we determined that Pom1, Tea4, and Dis2 were in close proximity in vivo (Figure 6E). BiFC signal was observed in pairs between Dis2, Pom1, and Pom1^{KD} with wild-type Tea4, but not Tea4^{SH3*}. However, Tea4^{SH3*} was able to form BiFC signals with Tea3, a cell end marker that associates

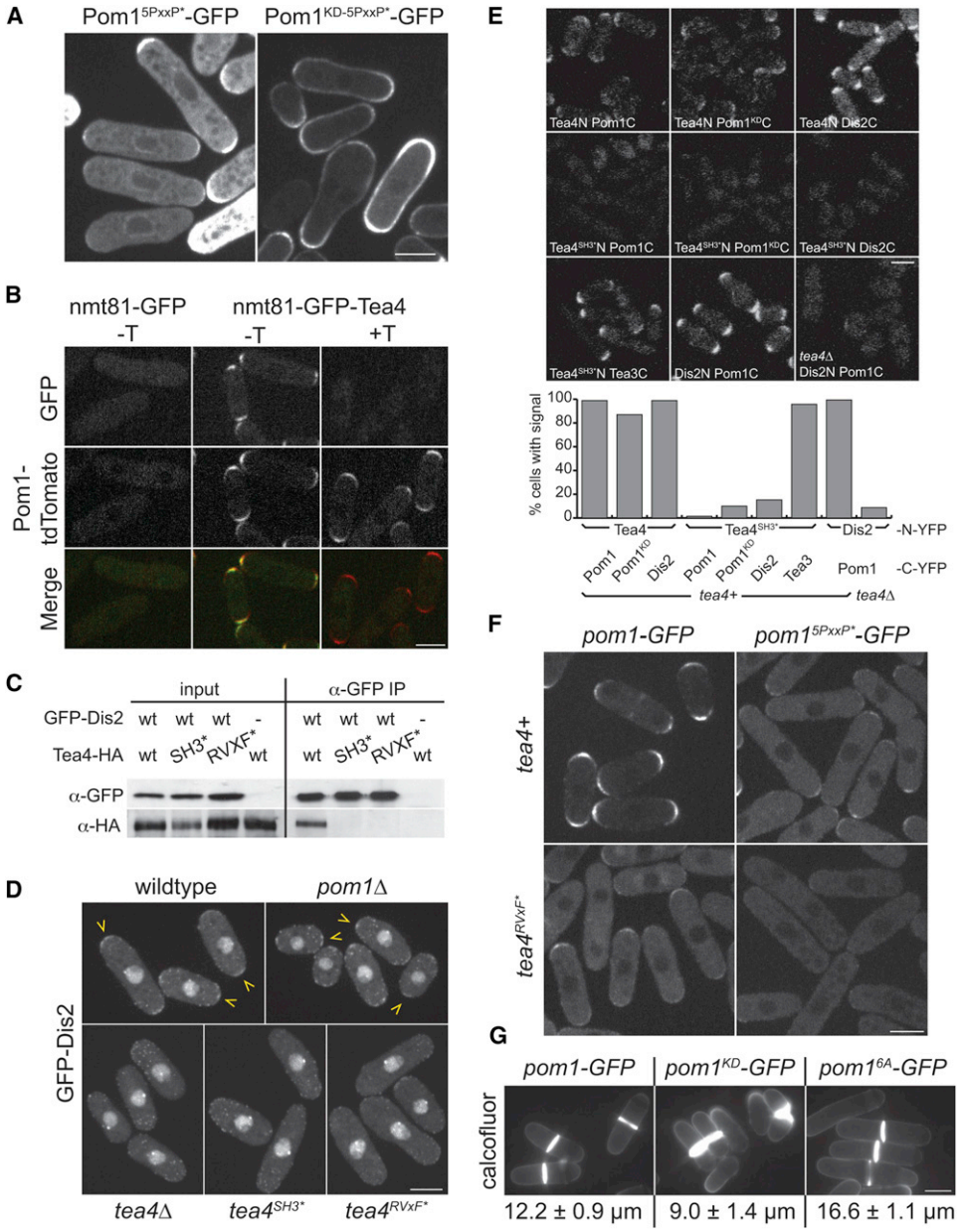

Figure 6. Tea4 and Dis2 Mediate Pom1 Dephosphorylation

(A) Localization of Pom1^{5PxxP*}-GFP and Pom1$^{KD\text{-}5PxxP*}$-GFP expressed from plasmids in *pom1Δ* cells.

(B) Repression of *nmt81-tea4-GFP* by addition of thiamine (T) leads to undetectable Tea4-GFP levels, yet correct Pom1-tdTomato localization. *nmt81-GFP* was expressed as control. GFP, Pom1-tdTomato and merge channels are shown.

(C) Coimmunoprecipitation of Tea4-HA with GFP-Dis2. Tea4 alleles are indicated at the top.

(D) Maximal projection of GFP-Dis2 localization in wild-type, *tea4Δ*, *tea4^{SH3*}*, *tea4^{RVxF*}*, and *pom1Δ* cells. Yellow arrowheads indicate cell tip localization. Note that other localizations to endocytic vesicles or the nucleus are not affected by *tea4* mutations (Alvarez-Tabares et al., 2007).

(E) BiFC experiment indicating proximity of Tea4, Dis2, and Pom1 in vivo. Top panels show reconstituted fluorescence between indicated full-length proteins expressed under endogenous promoter and tagged with either the N-terminal half (N), or the C-terminal half (C) of YFP. Bottom panel shows quantification of the percentage of cells with cortical signal (n > 100 for each sample).

(F) Localization of Pom1-GFP and Pom1^{5PxxP*}-GFP expressed under endogenous promoter in wild-type and *tea4^{RVxF*}* cells.

(G) Average length and standard deviation of calcofluor-stained septated cells of *pom1-GFP*, *pom1^{KD}-GFP*, and *pom1^{6A}-GFP* strains. Scale bars, 5 μm.

See also Figure S6.

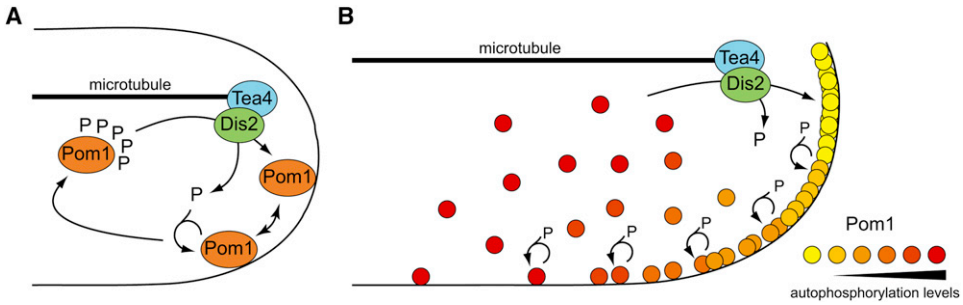

Figure 7. Model for the Formation of Cortical Pom1 Gradients

(A) Local dephosphorylation of Pom1, mediated by the Tea4-Dis2 PP1 pair, which is localized to cell tips through microtubule transport, permits association of Pom1 with the plasma membrane at cell tips. Pom1 then diffuses in the plane of the membrane. Autophosphorylation leads to Pom1 detachment from the membrane.

(B) Multiple autophosphorylation events may serve as a timer for shaping Pom1 gradients. After dephosphorylation and plasma membrane association, multiple rounds of autophosphorylation gradually increase the probability of Pom1 detaching from the membrane. Pom1 is shown in various shades of red indicating various degrees of autophosphorylation, from dephosphorylated (yellow) to fully phosphorylated (red).

with Tea1 and Tea4 (Snaith et al., 2005; data not shown). We also detected a BiFC signal between Dis2 and Pom1, which was dependent on *tea4*. These observations are consistent with the idea that Pom1, Tea4, and Dis2 interact at cell tips in vivo.

We investigated the effect of blocking the Tea4-Dis2 interaction on the localization of Pom1-GFP (Figure 6F): in *tea4*^{RVxF*} mutant cells, in which Dis2 but not Pom1 fails to bind mutant Tea4, Pom1-GFP was largely diffuse but retained some cell tip localization. In contrast, Pom1^{5PxxP*}-GFP failed to localize to the cell cortex in this background. This combination specifically blocks both the Tea4-Dis2 and Tea4-Pom1 interactions and mimics the *tea4*^{SH3*} mutant situation. Thus, efficient localization of Pom1 to the cell tip cortex requires both binding to Tea4 and interaction between Tea4 and the phosphatase Dis2, indicating that Tea4 bridges Pom1 with Dis2 to promote the dephosphorylation of Pom1 at cell tips.

Disruption of Pom1 Gradients Delays the Cell Cycle

We and others previously proposed that Pom1 gradients serve to couple cell length with mitotic entry (Martin and Berthelot-Grosjean, 2009; Moseley et al., 2009). We tested the effect of disturbing Pom1 gradients on cell length by investigating the phenotype of the *pom1*^{6A} mutant, which encodes an active kinase that spreads along the lateral cortex (see Figure 3). *pom1*^{6A} cells were highly elongated (Figure 6G) but did not show significant morphological defects. This contrasts with the *pom1*^{KD} cells, which are short, misshapen, and divide off center. Thus, *pom1*^{6A} appears to be a gain-of-function allele and displays a phenotype consistent with previously published data that ectopic localization of active Pom1 to the cell middle inhibits Cdr2 and delays mitotic commitment (Martin and Berthelot-Grosjean, 2009; Moseley et al., 2009). In conclusion, spreading of active Pom1 along the lateral cortex leads to cell cycle delay.

DISCUSSION

Concentration gradients pattern cells and organisms. Here, we have dissected with molecular details the mechanism of gradient formation of the DYRK family kinase Pom1. Pom1 gradient initiation relies on the local dephosphorylation of Pom1 at cell tips. This reaction is mediated by microtubule-deposited Tea4, which acts as a PP1 regulatory subunit, bridging the phosphatase Dis2 with its substrate Pom1. Dephosphorylation of Pom1 exposes a positively charged basic region that mediates plasma membrane association. At the membrane, Pom1 moves away from its site of association and autophosphorylates at multiple sites, in particular within its basic region. This autophosphorylation lowers its affinity to the membrane and promotes its detachment, limiting the lateral spreading of Pom1 along the membrane. In the cytoplasm, fast diffusion of Pom1 permits its encounter with Tea4 to initiate a new cycle of membrane association (Figure 7A). In summary we propose that a cycle of local dephosphorylation, lateral movement at the plasma membrane and autophosphorylation shapes Pom1 cortical gradients.

Our data clearly establish Tea4 as a bona fide PP1 regulatory subunit, as it binds both the phosphatase Dis2 and its substrate Pom1 and promotes Pom1 dephosphorylation. This function is likely shared with its homolog in *S. cerevisiae*, Bud14p, which serves as targeting subunit for the PP1 Glc7p (Knaus et al., 2005). However, exactly how a ternary complex forms between Tea4, Dis2, and Pom1 is unclear because both Pom1 and Dis2 require an intact SH3 ligand-binding interface for binding Tea4 and localizing to cell tips. Our data indicate that Tea4 binds Dis2 independently of Pom1 because Pom1 is not required for the localization of Dis2 to cell tips. This interaction requires both the RVxF motif and a nonclassical SH3 interaction (Dis2 does not contain PxxP repeats). Tea4 also binds Pom1 independently of Dis2, as Tea4^{RVxF*} still associates with Pom1, but not Dis2. This interaction occurs through classical SH3-PxxP contact. We suggest that the functional phosphatase unit is the Tea4-Dis2 dimer. In the absence of substrate, interaction through the RVxF site may be stabilized through a labile Dis2-Tea4 SH3 contact. However, upon Pom1 encounter this contact may be lost and Pom1 docked, transiently stabilizing the trimeric complex. Alternatively, Tea4 may dimerize, thus providing two independent SH3 domains for binding Pom1 and Dis2.

In vivo, Tea4 associates with Tea1, which is transported by microtubules and forms a subcortical network at cell tips (Bicho

et al., 2010; Martin et al., 2005; Tatebe et al., 2005). This may provide a microenvironment favorable to Pom1 dephosphorylation by enhancing the local concentration of Tea4, Pom1, and Dis2. Indeed, in *tea1Δ* cells, in which Tea4 fails to localize to cell tips, Pom1 localizes, albeit poorly, to the cell cortex (Celton-Morizur et al., 2006; Padte et al., 2006), indicating that the Tea4-Dis2 pair also promotes dephosphorylation of Pom1 in these conditions, though inefficiently. Thus, microtubules indirectly define the sites of Pom1 dephosphorylation.

Shaping the Pom1 Gradients

We and others previously proposed that the gradients of Pom1 serve to measure cell length by inhibiting the medial mitotic inducer Cdr2 (Martin and Berthelot-Grosjean, 2009; Moseley et al., 2009). Consistent with this model, disruption of Pom1 gradients using a nonphosphorylatable but active Pom1 allele ($Pom1^{6A}$) delays cell cycle progression, similar to *cdr2Δ*. One postulate of this model is that the shape of Pom1 gradients should be independent of cell length itself. Our data suggest that, upon plasma membrane association, gradient shape is controlled by two competing activities: lateral movement at the membrane will enhance Pom1 dispersal and promote the formation of a shallow gradient. The lateral movement we show is consistent with diffusion. In contrast, autophosphorylation will favor Pom1 detachment from the membrane and, thus, the formation of a steep gradient. The multiplicity of autophosphorylation sites within the basic region, which likely require sequential autophosphorylation events, may provide a "timer" function affording time for diffusion within the membrane before detachment (Figure 7B). The rate of movement of Pom1 at the plasma membrane appears sufficiently slow to allow the Pom1 concentration gradients to be maintained. Slow lateral mobility of both lipids and proteins has also been observed in the plasma membrane of the budding yeast (Greenberg and Axelrod, 1993; Valdez-Taubas and Pelham, 2003). Thus, the precise shape of the gradients will be defined by the rate of Pom1 lateral movement at the membrane and the time required for autophosphorylation.

Pom1 activity levels may provide a potential regulatory switch for modulating gradient shapes. Interestingly, Bähler and Nurse (2001) described that Pom1 kinase activity is not constant through the cell cycle but appears to increase through G2. This finding is somewhat contradictory with the model that local medial Pom1 activity levels are at their lowest at that time. Our findings can reconcile these two findings: the global increase in Pom1 activity may promote faster detachment of Pom1 from the membrane and formation of steeper gradients in late G2 cells. Thus, paradoxically, higher global Pom1 activity may contribute to reducing its activity at the cell middle by lowering its medial concentration.

If gradient shape is indeed modulated by Pom1 global activity, it will be important to define what controls this variation in activity. Does Pom1 activity increase in response to cell cycle progression itself? If so it may point toward a feedback system, where Pom1 does not provide an absolute measure of cell length but measures this length in a subjective cell cycle context-dependent manner. Quantitative modeling of Pom1 gradients will be necessary to define whether and how variation in Pom1 activity contributes to shaping them. Our molecular dissection of Pom1 gradients now provides the framework for this quantitative analysis.

Mechanics and Function of Autophosphorylation

Our data show that wild-type Pom1 cannot rescue the localization of inactive Pom1. The simplest interpretation of these results is that Pom1 undergoes intramolecular autophosphorylation events. An alternative possibility is that autophosphorylation events occur in *trans* between distinct Pom1 molecules but that wild-type and inactive Pom1 are blind to each other. Although, to our knowledge, no data exist to distinguish between these two possibilities, evidence suggests that Pom1 associates in large complexes. First, Pom1 forms high molecular weight complexes in biochemical fractionation (Bähler and Nurse, 2001). Second, clusters of Pom1 are detected at the membrane (see Figure 1A). Finally, in backgrounds where Pom1 associates weakly with the plasma membrane, such as the $Pom1^{1A}$-$Pom1^{3A}$ alleles, Pom1 forms defined domains of membrane association (Figure S6), suggesting a certain amount of cooperativity between distinct Pom1 molecules to associate at the membrane.

Besides the autophosphorylation sites in the basic region, mass spectrometry identified 39 other sites spread mostly in the noncatalytic regions of Pom1, of which all or only a subset may be phosphorylated on each Pom1 molecule. We note that most of these sites are significantly different from the DYRK consensus previously defined. What is the role of these additional sites? First, autophosphorylation at these sites may further help detach Pom1 from the membrane, similar to the six we characterized. Alternatively, autophosphorylation at these sites may underlie a second function, e.g., modulating Pom1 activity. Current evidence suggests that Pom1 is active at the cell cortex where Cdr2 localizes. Indeed, membrane-associated $Pom1^{6A}$ strongly delays mitotic entry. In contrast, cytoplasmic Pom1 in *tea4Δ* cells only causes a modest delay (unpublished data). Although substrate localization and accessibility may underlie this difference, it is also possible that Pom1 is less active in its fully autophosphorylated cytoplasmic state than its membrane-associated state. Finally, these autophosphorylation sites may also influence other Pom1 functions in cell morphogenesis or septum positioning.

Additional Spatial Cues for Pom1 Localization

The data and model presented above propose that Tea4 is the spatial cue for the formation of membrane-associated Pom1 gradients. (However, we note that Pom1 can localize to the septum independently of Tea4.) Indeed, we show that mislocalization of Tea4 is sufficient to initiate the formation of an ectopic Pom1 gradient. However, it is clear that other factors contribute to Pom1 localization. Although ectopic Tea4 was able to recruit Pom1 to the plasma membrane, it was unable to recruit it to internal membranes: the Ppc89-Tea4 fusion was also localized to the SPB, but Pom1 was not recruited to the nuclear membrane. Similar experiments conducted with a SPB component Sad1-Tea4 fusion confirmed this result (data not shown). Thus, the plasma membrane may be the only permissive membrane for Pom1 binding. In addition we noted that dephosphorylated Pom1 alleles and in particular partly dephosphorylated alleles

(such as Pom1^{1A}-Pom1^{3A}) show a preferential cortical localization to cell tips even in *tea4Δ* cells. Similarly, Pom1 shows preferential tip cortex localization in *tea1Δ* cells in which Tea4 is homogeneously distributed (Celton-Morizur et al., 2006; Padte et al., 2006). This preference may be conferred by membrane curvature, specific lipid composition of the plasma membrane at cell ends, or as yet uncharacterized membrane proteins.

Dynamic Maintenance of Cortical Gradients

Intracellular gradients are important for cell patterning. Yet, the mechanisms for gradient formation are generally not well described. Although large-scale gradients that pattern organisms during development, such as the Bicoid or Decapentaplegic gradients, reaching across hundreds of microns, rely on local translation and degradation (Wartlick et al., 2009), these second-order reactions are too slow for the formation of small-scale intracellular gradients. In contrast, intracellular gradients, such as the Ran-GTP gradient around chromatin or the bacterial polar MinCD gradient, are proposed to self-organize through autoregulatory feedbacks (Fuller, 2010; Lutkenhaus, 2007). One general feature is that these gradients are not static systems but are dynamically maintained by a constant flow of proteins cycling through distinct stages of membrane/organelle association and protein modification. Conceptually similar flow models serve for the kinetic polarization of membranes through endocytic recycling in migrating cells or budding yeast (Bretscher, 1996; Valdez-Taubas and Pelham, 2003). Our work now defines a detailed molecular mechanism for one such flow model.

Parallels with the MinCD gradient, where the MinD ATPase forms gradients from the ends of bacterial cells recruiting the division inhibitor MinC (Lutkenhaus, 2007), are particularly intriguing: both MinCD and Pom1 form cortical gradients and function in sensing cell length and regulating cell division. Moreover, these gradients are shaped by first-order reactions through endogenous enzymatic activity, where this activity promotes detachment from the membrane. The strategic similarities used by these unrelated proteins in distinct phyla suggest that the mechanisms we have defined may represent a general blueprint for building gradients along intracellular structures.

EXPERIMENTAL PROCEDURES

Detailed methods, including strain list (Table S1), are described in the Supplemental Information.

Mutants and Construct Information

The mutations introduced in the *tea4^{SH3*}* and *tea4^{RVxF*}* alleles are W155A-W156A and V223A-F225A, respectively. All mutations introduced in *pom1* are indicated in Figure S2 and Figure S5, except for *pom1^{KD}*, which is K728R (Bähler and Nurse, 2001). The Ppc89-GFP-Tea4 fusion was obtained by fusing in this order and in frame the three ORFs without stop codons in a pRIP81 plasmid. This fusion contains a small AGAGAG linker between GFP and Tea4. After linearization, this plasmid was then integrated at the *ura4* locus. Thus, this construct is present as sole copy in the cell under control of the weak *nmt* promoter.

Microscopy and Quantification

Unless stated otherwise, all images are two-dimensional maximum intensity projections of the three medial sections of spinning-disk confocal images, except the BiFC experiments, which are maximum intensity projections of the entire cell volume of laser-scanning confocal images. Except where stated, all images are of GFP-tagged gene products integrated as sole copy at the endogenous locus and expressed under endogenous promoter. All measurements were performed in ImageJ on images taken in identical conditions. We note that our measurements of fluorescence distribution were only corrected for background values and, thus, serve primarily as illustration of the images shown.

Protein-Lipid Binding Assays

Protein-lipid overlay assays were performed using lipid strips purchased from Echelon Inc., essentially according to manufacturer's protocol. We used MBP-Pom1 rather than GST-Pom1 because we found that GST alone bound some lipids with significant affinity. Recombinant Pom1 fragments bearing a functional kinase domain were found to be autophosphorylated in the bacterial cell. For all experiments we used 0.5 μg/ml of recombinant protein and performed control binding reactions in identical conditions in parallel. We reproducibly found that dephosphorylated Pom1 or the Pom1$_{1–699}$ fragment bound both lipids and membrane with higher affinity than autophosphorylated forms or MBP alone. The scans of the lipid strips shown have not been modified in any way.

SUPPLEMENTAL INFORMATION

Supplemental Information includes Extended Experimental Procedures, six figures, and one table and can be found with this article online at doi:10.1016/j.cell.2011.05.014.

ACKNOWLEDGMENTS

We would like to thank Patrice Waridel and Manfredo Quadroni at the Protein Analysis Facility for the mass spectrometry, Philippe Kircher for technical help, Jürg Bähler, Iain Hagan, and Stuart MacNeill for strains and reagents, Yves Barral, Felipe Bendezú, and Richard Benton for comments on the manuscript, and all members of the lab for advice and discussion. O.H. was supported by a Human Frontiers Science Program (HFSP) long-term fellowship (LT00595/2005-L) and K.K. by a Roche research fellowship (67-2008). Research in S.G.M.'s laboratory is supported by a Swiss National Science Foundation Professorship grant (PP00A-114936), an HFSP Career Development Award (CDA0016/2008), and a European Research Council Starting Grant (260493). We also extend our thanks to the Center for Integrative Genomics at the University of Lausanne, where a large part of this work was conducted, for generous support.

Received: December 22, 2010
Revised: March 23, 2011
Accepted: May 4, 2011
Published: June 23, 2011

REFERENCES

Almonacid, M., Moseley, J.B., Janvore, J., Mayeux, A., Fraisier, V., Nurse, P., and Paoletti, A. (2009). Spatial control of cytokinesis by Cdr2 kinase and Mid1/anillin nuclear export. Curr. Biol. *19*, 961–966.

Alvarez-Tabarés, I., Grallert, A., Ortiz, J.M., and Hagan, I.M. (2007). *Schizosaccharomyces pombe* protein phosphatase 1 in mitosis, endocytosis and a partnership with Wsh3/Tea4 to control polarised growth. J. Cell Sci. *120*, 3589–3601.

Aranda, S., Laguna, A., and de la Luna, S. (2011). DYRK family of protein kinases: evolutionary relationships, biochemical properties, and functional roles. FASEB J. *25*, 449–462.

Bähler, J., and Nurse, P. (2001). Fission yeast Pom1p kinase activity is cell cycle regulated and essential for cellular symmetry during growth and division. EMBO J. *20*, 1064–1073.

Bähler, J., and Pringle, J.R. (1998). Pom1p, a fission yeast protein kinase that provides positional information for both polarized growth and cytokinesis. Genes Dev. *12*, 1356–1370.

Bicho, C.C., Kelly, D.A., Snaith, H.A., Goryachev, A.B., and Sawin, K.E. (2010). A catalytic role for Mod5 in the formation of the Tea1 cell polarity landmark. Curr. Biol. *20*, 1752–1757.

Bretscher, M.S. (1996). Getting membrane flow and the cytoskeleton to cooperate in moving cells. Cell *87*, 601–606.

Campbell, L.E., and Proud, C.G. (2002). Differing substrate specificities of members of the DYRK family of arginine-directed protein kinases. FEBS Lett. *510*, 31–36.

Celton-Morizur, S., Racine, V., Sibarita, J.B., and Paoletti, A. (2006). Pom1 kinase links division plane position to cell polarity by regulating Mid1p cortical distribution. J. Cell Sci. *119*, 4710–4718.

Chang, F., and Martin, S.G. (2009). Shaping fission yeast with microtubules. Cold Spring Harb. Perspect. Biol. *1*, a001347.

Fuller, B.G. (2010). Self-organization of intracellular gradients during mitosis. Cell Div. *5*, 5.

Greenberg, M.L., and Axelrod, D. (1993). Anomalously slow mobility of fluorescent lipid probes in the plasma membrane of the yeast *Saccharomyces cerevisiae*. J. Membr. Biol. *131*, 115–127.

Himpel, S., Tegge, W., Frank, R., Leder, S., Joost, H.G., and Becker, W. (2000). Specificity determinants of substrate recognition by the protein kinase DYRK1A. J. Biol. Chem. *275*, 2431–2438.

Huang, Y., Chew, T.G., Ge, W., and Balasubramanian, M.K. (2007). Polarity determinants Tea1p, Tea4p, and Pom1p inhibit division-septum assembly at cell ends in fission yeast. Dev. Cell *12*, 987–996.

Kerppola, T.K. (2006). Visualization of molecular interactions by fluorescence complementation. Nat. Rev. Mol. Cell Biol. *7*, 449–456.

Knaus, M., Cameroni, E., Pedruzzi, I., Tatchell, K., De Virgilio, C., and Peter, M. (2005). The Bud14p-Glc7p complex functions as a cortical regulator of dynein in budding yeast. EMBO J. *24*, 3000–3011.

Koukou, A.I., Tsoukatos, D., and Drainas, C. (1990). Effect of ethanol on the phospholipid and fatty acid content of *Schizosaccharomyces pombe* membranes. J. Gen. Microbiol. *136*, 1271–1277.

Lochhead, P.A., Sibbet, G., Morrice, N., and Cleghon, V. (2005). Activation-loop autophosphorylation is mediated by a novel transitional intermediate form of DYRKs. Cell *121*, 925–936.

Lutkenhaus, J. (2007). Assembly dynamics of the bacterial MinCDE system and spatial regulation of the Z ring. Annu. Rev. Biochem. *76*, 539–562.

Martin, S.G., and Berthelot-Grosjean, M. (2009). Polar gradients of the DYRK-family kinase Pom1 couple cell length with the cell cycle. Nature *459*, 852–856.

Martin, S.G., McDonald, W.H., Yates, J.R., III, and Chang, F. (2005). Tea4p links microtubule plus ends with the formin for3p in the establishment of cell polarity. Dev. Cell *8*, 479–491.

Mata, J., and Nurse, P. (1997). tea1 and the microtubular cytoskeleton are important for generating global spatial order within the fission yeast cell. Cell *89*, 939–949.

Morrell, J.L., Nichols, C.B., and Gould, K.L. (2004). The GIN4 family kinase, Cdr2p, acts independently of septins in fission yeast. J. Cell Sci. *117*, 5293–5302.

Moseley, J.B., Mayeux, A., Paoletti, A., and Nurse, P. (2009). A spatial gradient coordinates cell size and mitotic entry in fission yeast. Nature *459*, 857–860.

Padte, N.N., Martin, S.G., Howard, M., and Chang, F. (2006). The cell-end factor pom1p inhibits mid1p in specification of the cell division plane in fission yeast. Curr. Biol. *16*, 2480–2487.

Snaith, H.A., Samejima, I., and Sawin, K.E. (2005). Multistep and multimode cortical anchoring of tea1p at cell tips in fission yeast. EMBO J. *24*, 3690–3699.

Tatebe, H., Shimada, K., Uzawa, S., Morigasaki, S., and Shiozaki, K. (2005). Wsh3/Tea4 is a novel cell-end factor essential for bipolar distribution of Tea1 and protects cell polarity under environmental stress in *S. pombe*. Curr. Biol. *15*, 1006–1015.

Tatebe, H., Nakano, K., Maximo, R., and Shiozaki, K. (2008). Pom1 DYRK regulates localization of the Rga4 GAP to ensure bipolar activation of Cdc42 in fission yeast. Curr. Biol. *18*, 322–330.

Valdez-Taubas, J., and Pelham, H.R. (2003). Slow diffusion of proteins in the yeast plasma membrane allows polarity to be maintained by endocytic cycling. Curr. Biol. *13*, 1636–1640.

Wartlick, O., Kicheva, A., and González-Gaitán, M. (2009). Morphogen gradient formation. Cold Spring Harb. Perspect. Biol. *1*, a001255.

Cell

EXTENDED EXPERIMENTAL PROCEDURES

Yeast Strains, Media, and Genetic Methods

Standard methods for *S. pombe* media and genetic manipulations were used throughout. Generally, for imaging, length measurements and biochemistry experiments, cells were grown in synthetic Edinburgh minimal medium (EMM) with appropriate supplements. For induction of *pom1-GFP* expression under *nmt* promoter in the pREP41 plasmid, cells were grown for 21-23h at 25°C in EMM medium lacking thiamine, except for strong overexpression where cells were grown for 24h at 30°C. *GFP*, *tea4-GFP* and *ppc89-GFP-tea4* under the weak *nmt* promoter integrated at the *ura4* locus were induced to steady-state levels for over 24h at 30°C in EMM medium lacking thiamine. Repression of *tea4-GFP* under the weak *nmt* promoter was done by growing cells in presence of 15μM thiamine for > 24h at 30°C.

All strains used in this study are listed in Table S1. Tagged and deletion strains were constructed by using a PCR-based approach (Bähler et al., 1998) and confirmed by PCR. Template for tdTomato and BiFC tagging were used as published (Akman and MacNeill, 2009; Snaith et al., 2005). Integration of mutant alleles at the endogenous genomic locus was performed through a two-step procedure: the wild-type copy was first replaced by a *ura4+* cassette amplified by PCR with 100-mer oligos containing homology to the flanking regions of the fragment to be deleted. This cassette was then further replaced by a mutant gene fragment and selected on 5-FOA medium.

Molecular Biology and Yeast Two-Hybrid Analysis

All plasmids were constructed using standard molecular biology techniques. In general, genes or gene fragments were cloned after PCR from genomic DNA with primers containing 5′ extensions with specific restriction sites. Details of the primers and restriction sites used are available upon request. All Pom1 expression plasmids were generated in the pREP41-GFP backbone (Craven et al., 1998). PCR-based site-directed mutagenesis was performed essentially as described. All plasmids were fully sequenced.

Two-hybrid assays were performed by co-transformation of appropriate pGAD and pGBD plasmids in AH109 host strain (Clontech). Interaction was assessed by growth on SD medium lacking histidine. All pGAD-tea4 constructs used interacted with pGBD-tea1 and pGBD-for3 used as positive controls (Martin et al., 2005).

Microscopy

Imaging was performed at room temperature on live cells, except where specified, on a PerkinElmer spinning disk microscope, as previously described (Martin and Berthelot-Grosjean, 2009), except for the BiFC experiments. Stacks of z-series confocal sections were acquired at 0.3 μm intervals with the Volocity software and images were rendered by two-dimensional maximum intensity of the 3 medial sections, unless stated otherwise. Figures were prepared with Adobe Photoshop CS5 and Adobe Illustrator CS5. FRAP experiments were performed on the same setup using the PerkinElmer photokinesis module. ROI were bleached with 12 repetitive scans. For Figure 4, post-bleach images were acquired at 5 s intervals for the first 60 s followed by 10 s intervals for the next 140 s and finally 30 s intervals for the last 600 s to minimize bleaching during image acquisition. For Figure 1, post-bleach images were acquired at regular intervals. The BiFC images were acquired on a Zeiss laser-scanning LSM 510 Meta confocal microscope. Except where stated all images are of GFP-tagged gene products integrated as sole copy at the endogenous locus and expressed under endogenous promoter. For imaging Pom1-GFP in *orb* mutants (Figure S1), 5ml exponential cultures were centrifuged at 3000 rpm for 2min, resuspended in −20°C methanol and fixed for 10min at −20°C; cells were then washed 3 times in PBS. Cell length measurements were performed on calcofluor (Sigma)-stained septated cells.

Inhibition of Pom1-as1 was done with 1NM-PP1 (Calbiochem) used at a final concentration of 20 μM from a 10mM stock solution in DMSO and added in YE medium. To follow the same cells before and after inhibitor addition, these experiments were performed in homemade PDMF channels mounted on coverslips. Cycloheximide (Sigma) was used at 0.1mg/ml final concentration.

Fluorescence Quantification

All measurements and calculations were performed in ImageJ and MS_Excel, respectively. FRAP quantification was performed as previously described (Martin and Chang, 2006). Time constants were estimated by the intersection of the curve with a line at half-maximal recovery. For whole-cell quantification of the distribution of Pom1-GFP in Figure 1, a sum projection of spinning disk confocal z-stacks of an individual cell was boxed and the ImageJ (10.2) "plot profile" tool was used to compress the fluorescence intensity into a one-dimensional line along the long axis of the cell, as described (Martin and Berthelot-Grosjean, 2009). For measurement of fluorescence intensity along the cell cortex or through the cell middle, a 5 pixel-wide line was drawn by hand at the periphery or along the long axis of the cell in a medial confocal section and fluorescence intensity obtained using the plot profile tool of ImageJ. Background correction was performed by subtracting the background fluorescence intensity measured just outside the cell examined. In Figure 1, data corresponding to 9 μm of the cell perimeter centered around the tip of the cell and 3 μm of the cell perimeter or 1.5 μm perpendicular to the cell periphery centered around Ppc89-GFP-Tea4 was acquired. For each channel, in order to compare fluorescence distribution and not absolute fluorescence levels, the integrated fluorescence intensity over the measured line was normalized to a value of one. We note that our measurements of fluorescence distribution were only corrected for background values and thus serve primarily as illustration of the images shown.

Coimmunoprecipitations and Electrophoresis

Extracts from yeast grown in EMM medium were prepared in CXS buffer (50 mM HEPES, pH 7.0, 20mM KCl, 1mM MgCl2, 2mM EDTA, pH 7.5. and protease inhibitor cocktail) by grinding in liquid nitrogen with a mortar and pestle. After thawing, NaCl and Triton X-100 were added to final concentrations of 150mM and 0.1% respectively. For immunoprecipitations, 150 μl soluble extract was added to 20 μl sheep anti-mouse magnetic Dynabead slurry (Dynal) pre-bound to 2 mg monoclonal anti-GFP antibodies (Roche), and incubated for 2h at 4°C. Magnetic Dynabeads were then washed twice with CXS 150mM NaCl 0.1% Triton X-100 then twice with CXS 75mM NaCl 0.1% Triton X-100 and finally twice with CXS 75mM NaCl. Immunoprecipitated material was then recovered by boiling Dynabeads in 30 μl SDS sample buffer for 5 min at 95°C.

Standard protocols were used for SDS-PAGE and Western blot analysis. Antibodies used on Western blots were: mouse monoclonal anti-HA (HA.11; Covance), anti-GFP (Roche), anti-MBP (Cell Signaling) and anti-GST (Sigma). Silver staining was done using the SilverSNAP Stain Kit II (Pierce).

Recombinant Protein Expression and In Vitro Assays

MBP-Pom1 and GST-Pom1 fusion proteins were expressed in BL21 cells and purified with amylose resin (NEB) or glutathione sepharose 4B (GE Healthcare) columns according to manufacturers' protocols. 6His-Cdr2$_{423-532}$ was expressed and purified as described (Martin and Berthelot-Grosjean, 2009).

Kinase assays, were performed in 30mM Tris, 100mM NaCl, 10mM $MgCl_2$, 1mM EGTA, 10% glycerol, 20 μM ATP and 2 μCi [^{32}P] ATP (PerkinElmer #BLU502A250UC) with equivalent amounts of GST-Pom1, GST-Pom1^{KD} and GST-pom1^{6A} in a 15 μl final volume reaction. After a 30 min incubation at 30°C, the reaction was stopped by boiling in sample buffer and analyzed by SDS–PAGE. ^{32}P-incorporation was detected in a phosphorimager.

For phosphatase assays, equivalent amounts of GST-Pom1, GST-Pom1^{KD} and GST-pom1^{6A} were treated with 3,75U of PP1 (NEB #P0754S) in 1X PMP Buffer (NEB) supplemented with 1mM $MnCl_2$ and incubated at 30°C for 1h.

Phosphorylation Analysis of Pom1 by LC-MS/MS

Bands corresponding to phosphorylated recombinant GST-Pom1 were excised from SDS-PAGE gel and digested, as described (Shevchenko et al., 1996; Wilm et al., 1996), with sequencing-grade trypsin (Promega), chymotrypsin (Roche), Lys-C (Roche) or Glu-C (Sigma-Aldrich). Extracted peptides were analyzed on a hybrid LTQ Orbitrap Velos mass spectrometer (Thermo Fisher Scientific, Bremen, Germany) interfaced to an Ultimate 3000 RSLC nano HPLC system (Dionex, Olten, Switzerland). In data-dependent acquisition controlled by Xcalibur 2.1 software (Thermo Fisher Scientific), the 15 most intense precursor ions detected in the full MS survey performed in the Orbitrap (range 300-1700 m/z, resolution 30′000 at m/z 400) were selected and fragmented. Only precursors with a charge higher than one were selected for HCD fragmentation and fragment ions were analyzed in the Orbitrap at a resolution of 7′500. From raw files, MS/MS spectra were de-isotoped, deconvoluted and exported as mgf files (Mascot Generic File, text format) using MascotDistiller 2.3.2 (Matrix Science, London, UK). In a parallel experiment, phosphopeptides of Pom1 were enriched on a TiO_2 column (Larsen et al., 2005) after Lys-C digestion and analyzed by LC-MS/MS, in order to clarify some ambiguous phosphosite localization.

MS/MS spectra were analyzed using Mascot 2.2 (Matrix Science, London, UK). Mascot was set up to search the UNIPROT database (SWISSPROT + TrEMBL, www.expasy.org) restricted to *Schizosaccharomyces pombe* taxonomy (database release used was 15.12 of December, 15th 2009, 5′159 sequences after taxonomy filter). Trypsin (semi-specific cleavage at K,R, not before P), chymotrypsin (semi-specific cleavage at F,L;W,Y, not before P), Lys-C (semi-specific cleavage at K, not before P) or Glu-C (semi-specific cleavage at D,E, not before P), was used as the enzyme definition. Mascot was searched with a fragment ion mass tolerance of 0.02 Da, a parent ion tolerance of 10 ppm, allowing four missed cleavages. Iodoacetamide derivative of cysteine was specified in Mascot as a fixed modification. Deamidation of asparagine and glutamine, oxidation of methionine, and phosphorylation of serine, threonine and tyrosine were specified as variable modifications.

Combined analysis of trypsin, chymotrypsin, Lys-C and Glu-C datasets allowed the characterization of 41 phosphosites with 95.9% coverage of Pom1 sequence, using a Mascot ion score threshold of 14. Phosphorylation sites with ambiguous localization were noted as potential, when the difference between the top two Mascot ion scores of two alternative phosphorylation sites in the same peptide sequence was below 5. No peptide covering amino-acids 405 to 429, 436 to 445 and 482 to 487 could be observed in any of the four protease datasets. As these regions are rich in hydrophilic residues (S, T, K, R), the corresponding peptides were probably not retained on the C18 chromatographic column.

SUPPLEMENTAL REFERENCES

Akman, G., and MacNeill, S.A. (2009). MCM-GINS and MCM-MCM interactions in vivo visualised by bimolecular fluorescence complementation in fission yeast. BMC Cell Biol. *10*, 12.

Alvarez-Tabarés, I., Grallert, A., Ortiz, J.M., and Hagan, I.M. (2007). Schizosaccharomyces pombe protein phosphatase 1 in mitosis, endocytosis and a partnership with Wsh3/Tea4 to control polarised growth. J. Cell Sci. *120*, 3589–3601.

Bähler, J., and Pringle, J.R. (1998). Pom1p, a fission yeast protein kinase that provides positional information for both polarized growth and cytokinesis. Genes Dev. *12*, 1356–1370.

Bähler, J., Wu, J.Q., Longtine, M.S., Shah, N.G., McKenzie, A., III, Steever, A.B., Wach, A., Philippsen, P., and Pringle, J.R. (1998). Heterologous modules for efficient and versatile PCR-based gene targeting in *Schizosaccharomyces pombe.* Yeast *14*, 943–951.

Craven, R.A., Griffiths, D.J., Sheldrick, K.S., Randall, R.E., Hagan, I.M., and Carr, A.M. (1998). Vectors for the expression of tagged proteins in *Schizosaccharomyces pombe.* Gene *221*, 59–68.

Larsen, M.R., Thingholm, T.E., Jensen, O.N., Roepstorff, P., and Jørgensen, T.J. (2005). Highly selective enrichment of phosphorylated peptides from peptide mixtures using titanium dioxide microcolumns. Mol. Cell. Proteomics *4*, 873–886.

Martin, S.G., and Berthelot-Grosjean, M. (2009). Polar gradients of the DYRK-family kinase Pom1 couple cell length with the cell cycle. Nature *459*, 852–856.

Martin, S.G., and Chang, F. (2006). Dynamics of the formin for3p in actin cable assembly. Curr. Biol. *16*, 1161–1170.

Martin, S.G., McDonald, W.H., Yates, J.R., III, and Chang, F. (2005). Tea4p links microtubule plus ends with the formin for3p in the establishment of cell polarity. Dev. Cell *8*, 479–491.

Padte, N.N., Martin, S.G., Howard, M., and Chang, F. (2006). The cell-end factor pom1p inhibits mid1p in specification of the cell division plane in fission yeast. Curr. Biol. *16*, 2480–2487.

Shevchenko, A., Wilm, M., Vorm, O., and Mann, M. (1996). Mass spectrometric sequencing of proteins silver-stained polyacrylamide gels. Anal. Chem. *68*, 850–858.

Snaith, H.A., Samejima, I., and Sawin, K.E. (2005). Multistep and multimode cortical anchoring of tea1p at cell tips in fission yeast. EMBO J. *24*, 3690–3699.

Wilm, M., Shevchenko, A., Houthaeve, T., Breit, S., Schweigerer, L., Fotsis, T., and Mann, M. (1996). Femtomole sequencing of proteins from polyacrylamide gels by nano-electrospray mass spectrometry. Nature *379*, 466–469.

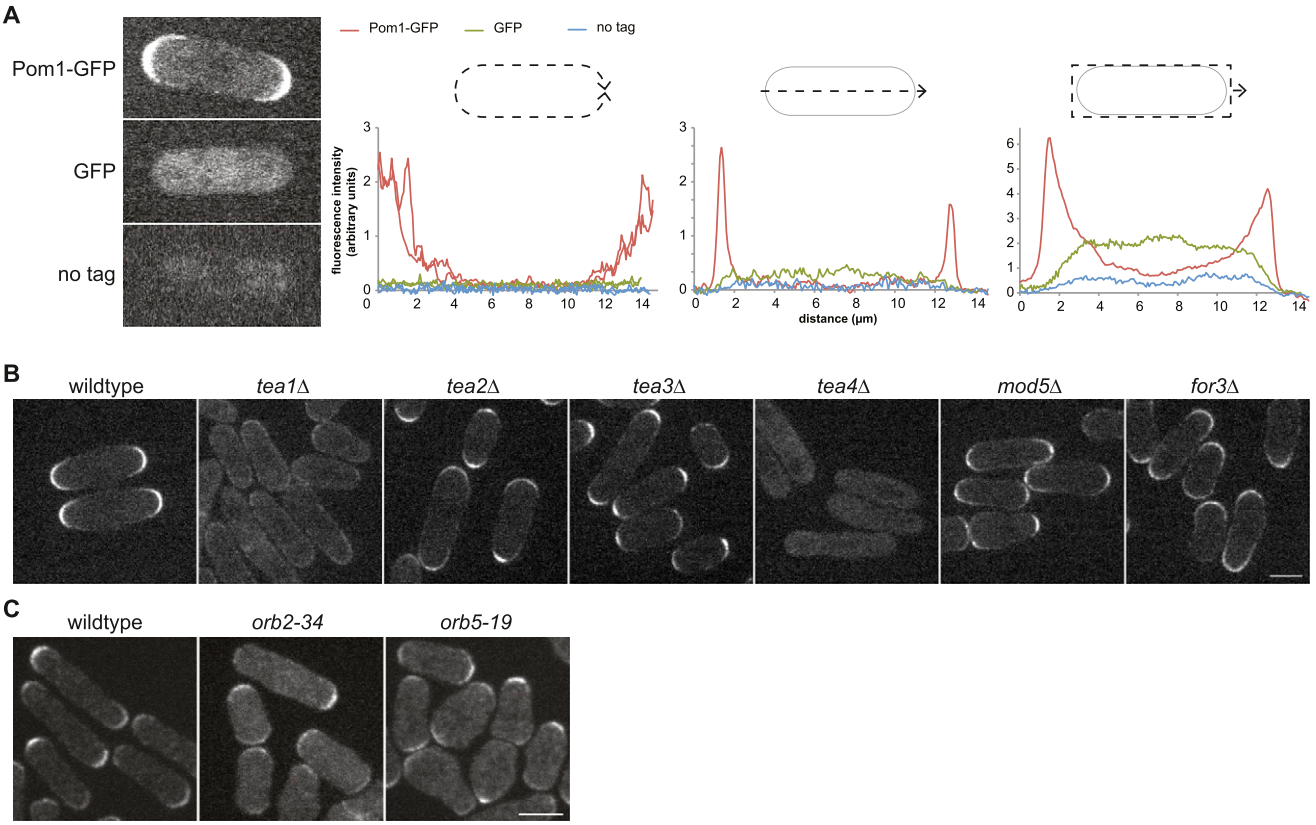

Figure S1. Pom1 Localization in Wild-Type Cells and in Polarity Mutants, Related to Figure 1

(A) Localization of Pom1-GFP and GFP, as well as background fluorescence intensity of unlabelled cells. Cells were imaged in identical conditions and a single medial confocal section is shown. The fluorescence intensity was measured along the periphery of each cell half (graph on the left) and across the cell length (middle graph), as in Figure 1A. The sum fluorescence intensity of the entire cell volume along the length of the cell is shown on the graph on the right. While neither GFP nor background signal are distributed in a graded pattern, Pom1-GFP forms cortical concentration gradients.

(B) Localization of Pom1-GFP in indicated genotypes in live cells grown at 30°C.

(C) Localization of Pom1-GFP in cells of indicated genotypes grown at the restrictive temperature of 36°C for 2h30 and fixed. Scale bars are 5μm.

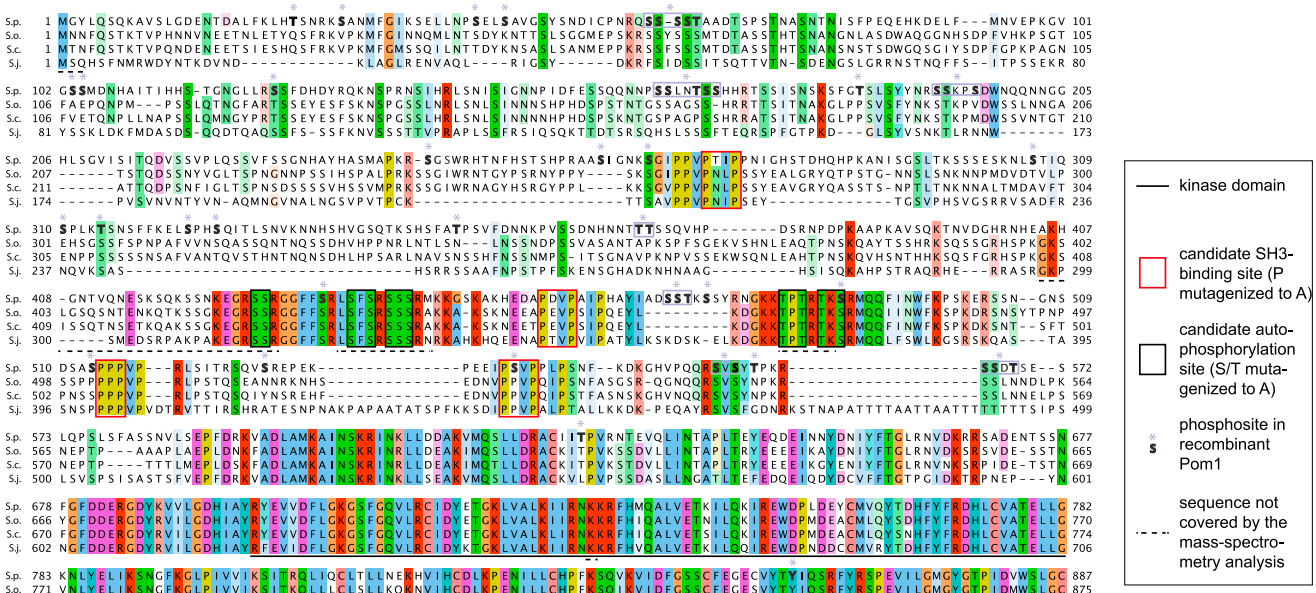

Figure S2. Alignment of Pom1 with Orthologs from Other *Schizosaccharomyces* Species, Related to Figure 2

Alignment of Pom1 orthologs in 4 *Schizosaccharomyces* species (S.p.: *pombe*, S.o.: *octosporus*, S.c.: *cryophobus*, S.j.: *japonicus*). The kinase domain is underlined. Serine/threonine residues mutated to alanine in the Pom1^{6A} allele are boxed in black. Proline residues mutated to alanine in the Pom1^{5PxxP*} allele are boxed in red. All phosphorylated residues identified by mass-spectrometry are in bold and highlighted by a purple asterisk. Purple boxes around some of these indicate that only one of the two or more boxed residues are phosphorylated, but that the exact phosphorylated residue could not be precisely resolved. Regions for which no peptides were recovered in the mass-spectrometry are underlined with a dashed line.

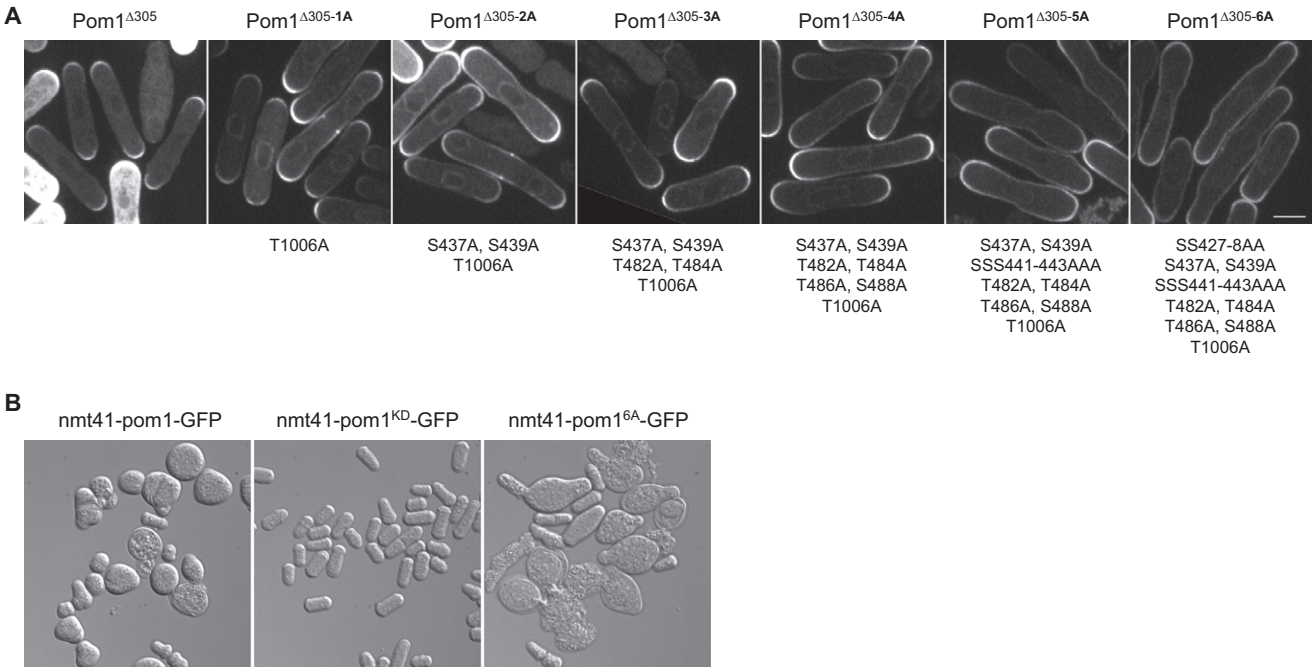

Figure S3. Mutation of Pom1 Autophosphorylation Sites Causes Progressive Cortical Spreading of Active Pom1, Related to Figure 3

(A) Localization of indicated Pom1-GFP alleles expressed from plasmids in *pom1Δ* cells. The corresponding mutations are indicated at the bottom. Note that all mutations were introduced in the N-terminal truncated $Pom1^{\Delta 305}$ allele, which lacks the first 305 amino acids not essential for localization. Scale bar is 5μm.

(B) Strong overexpression of wild-type or $Pom1^{6A}$-GFP, but not $Pom1^{KD}$-GFP leads to morphological defects. The constructs were expressed on plasmid under *nmt41* promoter and induced for 24h at 30°C. The cells were fixed in 70% EtOH.

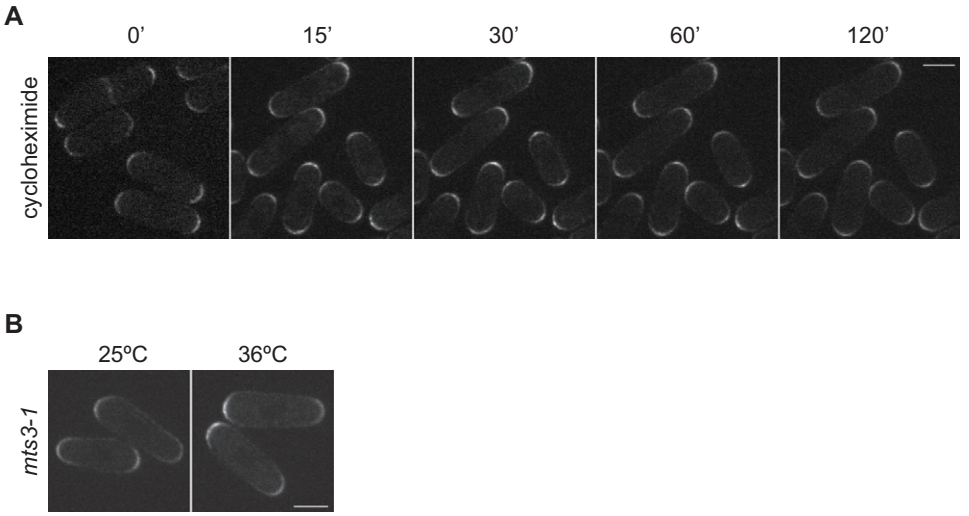

Figure S4. Pom1 Localization Is Not Controlled by Translation and Degradation, Related to Figure 4

(A) Localization of Pom1-GFP after indicated time in cycloheximide.

(B) Localization of Pom1-GFP in the thermosensitive *mts3-1* proteasome mutants grown at 25°C or 36°C for 2h30. Scale bars are 5μm.

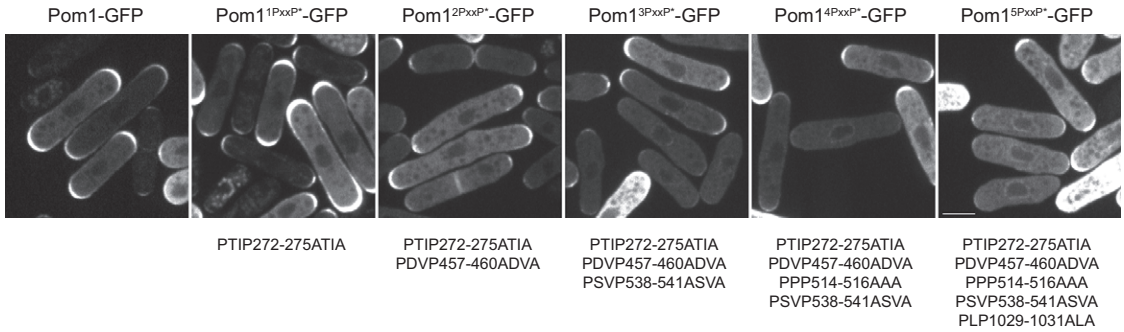

Figure S5. Mutation of PxxP Motifs Reduces Pom1 Localization to Cell Tips, Related to Figure 5

Localization of indicated Pom1-GFP alleles expressed from plasmids in *pom1Δ* cells. The corresponding mutations are indicated at the bottom. Scale bar is 5μm.

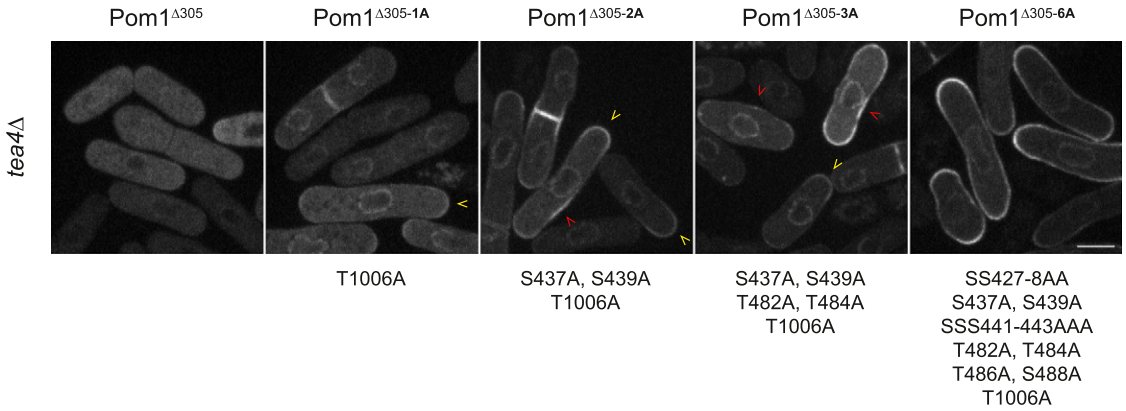

Figure S6. Mutation of Autophosphorylation Sites Bypasses the Need for Tea4 for Pom1 Localization to the Cell Periphery, Related to Figure 6

Localization of indicated Pom1-GFP alleles expressed from plasmids in *tea4Δ* cells. The corresponding mutations are indicated at the bottom. As in Figure S3, all mutations were introduced in the N-terminal truncated Pom1$^{\Delta 305}$ allele, which lacks the first 305 amino acids not essential for localization. Note that even mutation of few autophosphorylation sites is sufficient to restore partial localization of Pom1 to the cell periphery in *tea4Δ* cells. While these Pom1 alleles can localize anywhere around the periphery of the cell (red arrowheads), there appears to be a preference for cell tips (yellow arrowheads). Note that Pom1 does not appear to localize uniformly at the cortex, but forms domains of higher intensity. Scale bar is 5μm.

Table S1. *S. pombe* Strains Used in This Study, Related to Extended Experimental Procedures

Number	Genotype	Source
Figure 1		
YSM119	h- pom1-GFP-kanMX	(Bähler and Pringle, 1998)
YSM1276	h+ pom1-tomato-natMX tea4-GFP-kanMX ade6-M216 leu1-32 ura4-D18	This study
YSM1345	h+ pom1Δ::kanMK ade6-M216 leu1-32 ura4-D18 [pREP41-pom1-GFP]	This study
YSM1833	h+ pom1Δ::kanMX ade6-M216 leu1-32 ura4-D18 [pREP41-pom1^{KD}-GFP]	This study
YSM1672	tea4Δ::kanMX ura4-294::nmt81:ppc89-GFP-tea4-ura4+ pom1-tdTomato-natMX leu1-32	This study
Figure 2		
YSM1345	h+ pom1Δ::kanMX ade6-M216 leu1-32 ura4-D18 [pREP41-pom1-GFP]	This study
YSM1348	h+ pom1Δ::kanMX ade6-M216 leu1-32 ura4-D18 [pREP41-pom1Δ168-GFP]	This study
YSM1350	h+ pom1Δ::kanMX ade6-M216 leu1-32 ura4-D18 [pREP41-pom1Δ238-GFP]	This study
YSM1352	h+ pom1Δ::kanMX ade6-M216 leu1-32 ura4-D18 [pREP41-pom1Δ305-GFP]	This study
YSM1832	h+ pom1Δ::kanMX ade6-M216 leu1-32 ura4-D18 [pREP41-pom1Δ419-GFP]	This study
YSM1831	h+ pom1Δ::kanMX ade6-M216 leu1-32 ura4-D18 [pREP41-pom1Δ499-GFP]	This study
YSM1852	h+ pom1Δ::kanMX ade6-M216 leu1-32 ura4-D18 [pREP41-pom1$_{(305-510)}$-GFP]	This study
YSM1866	h+ pom1Δ::kanMX ade6-M216 leu1-32 ura4-D18 [pREP41-pom1$_{(419-499)}$-GFP]	This study
Figure 3		
YSM1344	h+ ade6-M216 leu1-32 ura4-D18 [pREP41-pom1-GFP]	This study
YSM1345	h+ pom1Δ::kanMX ade6-M216 leu1-32 ura4-D18 [pREP41-pom1-GFP]	This study
YSM1834	h+ ade6-M216 leu1-32 ura4-D18 [pREP41-pom1^{KD}-GFP]	This study
YSM1833	h+ pom1Δ::kanMX ade6-M216 leu1-32 ura4-D18 [pREP41-pom1^{KD}-GFP]	This study
YSM1844	h+ pom1Δ::kanMX ade6-M216 leu1-32 ura4-D18 [pREP41-pom1^{6A}-GFP]	This study
YSM1846	h+ ade6-M216 leu1-32 ura4-D18 [pREP41-pom1^{6A}-GFP]	This study

YSM119	h- pom1-GFP-kanMX	(Bähler and Pringle, 1998)
YSM1511	pom1^{KD}-GFP-kanMX	This study
YSM1849	pom1^{6A}-GFP-kanMX	This study
Figure 4		
YSM799	h+ pom1-as1-tomato-natMX ade6-M216 leu1-32 ura4-D18	This study
YSM119	h- pom1-GFP-kanMX	(Bähler and Pringle, 1998)
YSM1511	pom1^{KD}-GFP-kanMX	This study
YSM1849	pom1^{6A}-GFP-kanMX	This study
Figure 5		
YSM119	h- pom1-GFP-kanMX	(Bähler and Pringle, 1998)
YSM1511	pom1^{KD}-GFP-kanMX	This study
YSM1849	pom1^{6A}-GFP-kanMX	This study
YSM165	h- tea4Δ::kanMX pom1-GFP-kanMX ura4-	(Padte et al., 2006)
YSM1855	tea4Δ::kanMX pom1^{KD}-GFP-kanMX ade6-M210 leu1-32 ura4-D18	This study
YSM1851	tea4Δ::kanMX pom1^{6A}-GFP-kanMX ade6-M216 leu1-32 ura4-D18	This study
YSM1859	tea4^{SH3*} pom1-GFP-kanMX ade6-M210 leu1-32 ura4-D18	This study
YSM1808	tea4^{SH3*}-HA-kanMX pom1^{KD}-GFP-kanMX ade6- leu1- ura4-	This study
YSM1856	h+ tea4^{SH3*} pom1^{6A}-GFP-kanMX ade6-M216 leu1-32 ura4-D18	This study
Figure 6		
YSM1845	h+ pom1Δ::kanMX ade6-M216 leu1-32 ura4-D18 [pREP41-pom1^{5PxxP}*-GFP]	This study
YSM1847	h+ pom1Δ::kanMx ade6-M216 leu1-32 ura4-D18 [pREP41-pom1$^{KD\text{-}5PxxP*}$-GFP]	This study
YSM1794	tea4Δ::kanMX ura4-294::nmt81:GFP-ura4+ pom1-tdTomato-natMX leu1-32	This study
YSM1694	tea4Δ::kanMX ura4-294::nmt81:GFP-tea4-ura4+ pom1-tdTomato-natMX leu1-32	This study
YSM1184	h- dis2-NEGFP-ura4+ leu1-32 ura4-D18	(Alvarez-Tabares et al., 2007)

YSM1827	dis2-NEGFP-ura4+ tea4Δ ade6-M216 leu1-32 ura4-D18	This study
YSM1828	dis2-NEGFP-ura4+ tea4^{SH3*} ade6-M216 leu1-32 ura4-D18	This study
YSM1829	dis2-NEGFP-ura4+ tea4^{RVxF*} ade6-M216 leu1-32 ura4-D18	This study
YSM1711	dis2-NEGFP-ura4+ pom1Δ::kanMX leu1-32 ura4-D18	This study
YSM1771	tea4-YFP$_{Venus}$N173-natMX dis2-YFP$_{Venus}$C155-kanMX	This study
YSM1779	tea4-YFP$_{Venus}$N173-natMX pom1-YFP(Venus)C155-kanMX	This study
YSM1812	tea4-YFP$_{Venus}$N173-natMX pom1^{KD}-YFP$_{Venus}$C155-kanMX	This study
YSM1804	tea4^{SH3*}-YFP$_{Venus}$N173-natMX dis2-YFP$_{Venus}$C155-kanMX	This study
YSM1805	tea4^{SH3*}-YFP$_{Venus}$N173-natMX pom1-YFP$_{Venus}$C155-kanMX	This study
YSM1810	tea4^{SH3*}-YFP$_{Venus}$N173-natMX pom1^{KD}-YFP$_{Venus}$C155-kanMX	This study
YSM1803	tea4^{SH3*}-YFP$_{Venus}$N173-natMX tea3-YFP$_{Venus}$C155-kanMX	This study
YSM1774	dis2-YFP$_{Venus}$N173-natMX pom1-YFP$_{Venus}$C155-kanMX	This study
YSM1791	dis2-YFP$_{Venus}$N173-natMX pom1-YFP$_{Venus}$C155-kanMX tea4Δ::kanMX	This study
YSM119	h- pom1-GFP-kanMX	(Bähler and Pringle, 1998)
YSM1848	h- pom1^{5PxxP*}-GFP- kanMX ade6-M216 leu1-32 ura4-D18	This study
YSM1830	pom1-GFP-kanMX tea4^{RVxF*} ade6-M216 leu1-32 ura4-D18	This study
YSM1850	pom1^{5PxxP*}-GFP-kanMX tea4^{RVxF*} ade6-M216 leu1-32 ura4-D18	This study
YSM1511	pom1^{KD}-GFP-kanMX	This study
YSM1849	pom1^{6A}-GFP-kanMX	This study
Figure S1		
YSM119	h- pom1-GFP-kanMX	(Bähler and Pringle, 1998)
YSM1793	h+ ura4-294::nmt81:GFP-ura4+ leu1-32	This study
YSM1180	h- ade6-M210 leu1-32 ura4-D18	Lab stock
YSM813	h+ pom1-GFP-kanMX tea1Δ::ura4+ ade6- leu1- ura4-	(Padte et al., 2006)
YSM1857	h- pom1-GFP-kanMX tea2Δ::his3+	This study

YSM811	pom1-GFP-kanMX tea3Δ::kanMX	This study
YSM165	h- pom1-GFP-kanMX tea4Δ::kanMX ura4-	(Padte et al., 2006)
YSM1853	h+ pom1-GFP mod5Δ leu1-32	This study
YSM521	pom1-GFP-kanMX for3Δ::kanMX leu1-	This study
YSM1303	pom1-GFP-kanMX orb2-34	This study
YSM1304	pom1-GFP-KanMX orb5-19	This study
Figure S3		
YSM1352	h+ pom1Δ::kanMX ade6-M216 leu1-32 ura4-D18 [pREP41-pom1Δ305-GFP]	This study
YSM1451	h+ pom1Δ::kanMX ade6-M216 leu1-32 ura4-D18 [pREP41-pom1Δ305^{1A}-GFP]	This study
YSM1602	h+ pom1Δ::kanMX ade6-M216 leu1-32 ura4-D18 [pREP41-pom1Δ305^{2A}-GFP]	This study
YSM1614	h+ pom1Δ::kanMX ade6-M216 leu1-32 ura4-D18 [pREP41-pom1Δ305^{3A}-GFP]	This study
YSM1835	h+ pom1Δ::kanMX ade6-M216 leu1-32 ura4-D18 [pREP41-pom1Δ305^{5A}-GFP]	This study
YSM1837	h+ pom1Δ::kanMX ade6-M216 leu1-32 ura4-D18 [pREP41-pom1Δ305^{6A}-GFP]	This study
YSM1344	h+ ade6-M216 leu1-32 ura4-D18 [pREP41-pom1-GFP]	This study
YSM1834	h+ ade6-M216 leu1-32 ura4-D18 [pREP41-pom1^{KD}-GFP]	This study
YSM1846	h+ ade6-M216 leu1-32 ura4-D18 [pREP41-pom1^{6A}-GFP]	This study
Figure S4		
YSM119	h- pom1-GFP-kanMX	(Bähler and Pringle, 1998)
YSM1854	h+ pom1-GFP mts3-1 leu1-32	This study
Figure S5		
YSM1345	h+ pom1Δ::kanMX ade6-M216 leu1-32 ura4-D18 [pREP41-pom1-GFP]	This study
YSM1638	h+ pom1Δ::kanMX ade6-M216 leu1-32 ura4-D18 [pREP41-pom1^{1PxxP*}-GFP]	This study
YSM1639	h+ pom1Δ::kanMX ade6-M216 leu1-32 ura4-D18 [pREP41-pom1^{2PxxP*}-GFP]	This study
YSM1842	h+ pom1Δ::kanMX ade6-M216 leu1-32 ura4-D18 [pREP41-pom1^{3PxxP*}-GFP]	This study
YSM1843	h+ pom1Δ::kanMX ade6-M216 leu1-32 ura4-D18 [pREP41-pom1^{4PxxP*}-GFP]	This study
YSM1845	h+ pom1Δ::kanMX ade6-M216 leu1-32 ura4-D18 [pREP41-pom1^{5PxxP*}-GFP]	This study

Figure S6		
YSM1836	h+ tea4Δ::kanMX ade6-M216 leu1-32 ura4-D18 [pREP41-pom1Δ305N-GFP]	This study
YSM1838	h+ tea4Δ::kanMX ade6-M216 leu1-32 ura4-D18 [pREP41-pom1Δ305^{1A}-GFP]	This study
YSM1839	h+ tea4Δ::kanMX ade6-M216 leu1-32 ura4-D18 [pREP41-pom1Δ305^{2A}-GFP]	This study
YSM1840	h+ tea4Δ::kanMX ade6-M216 leu1-32 ura4-D18 [pREP41-pom1Δ305^{3A}-GFP]	This study
YSM1841	h+ tea4Δ::kanMX ade6-M216 leu1-32 ura4-D18 [pREP41-pom1Δ305^{6A}-GFP]	This study